OCEAN RENEWABLE POWER COMPANY
FINAL TECHNICAL REPORT, DE-EE0006397
ADVANCED ENERGY HARVESTING CONTROL SCHEMES FOR MARINE RENEWABLE ENERGY DEVICES

PRINCIPLE INVESTIGATORS:

- *JARLATH MCENTEE, VICE PRESIDENT – ENGINEERING & CHIEF TECHNOLOGY OFFICER*
- *BRIAN POLAGYE, PH.D., ASSOCIATE PROFESSOR, MECHANICAL ENGINEERING, UNIVERSITY OF WASHINGTON*
- *BRIAN FABIEN, PH.D., PROFESSOR, MECHANICAL ENGINEERING, UNIVERSITY OF WASHINGTON*
- *JIM THOMSON, PH.D., PRINCIPAL OCEANOGRAPHER, APPLIED PHYSICS LABORATORY, UNIVERSITY OF WASHINGTON*
- *LEVI KILCHER, PH.D., OCEAN ENERGY RESEARCH SCIENTIST, WIND TECHNOLOGY CENTER, NATIONAL RENEWABLE ENERGY LABORATORY*

March 31, 2016

Ocean Renewable Power Company, LLC
66 Pearl Street, Suite 301
Portland, ME 04101
Phone (207) 772-7707
www.orpc.co

Acknowledgment:
This report is based upon work supported by the U. S. Department of Energy under Award No. DE-EE0006397.

Disclaimer:
Any findings, opinions, and conclusions or recommendations expressed in this report are those of the author(s) and do not necessarily reflect the views of the Department of Energy.

CONTENTS

List of Acronyms

ADCP	Acoustic Doppler Current Profiler
ADV	Acoustic Doppler Velocimeter
AEP	Annualized Energy Production
BP	budget period
CFD	computational fluid dynamics
DOE	US Department of Energy
EC	electronics cabinet
EEM	electromechanical emulation machine
E_{Loss}	energy loss metric
FEA	finite element analysis
IPM	Intellectual Property Management Plan
LCOE	levelized cost of electricity
MHK	marine hydrokinetic
NREL	National Renewable Energy Laboratory
ORPC	Ocean Renewable Power Company
PID	Proportional plus Integral and Derivative
PLC	Programmable logic controller
PMP	Project Management Plan
PMSG	permanent magnet synchronous generator
PWR	Power to Weight Ratio
RPM	revolutions per minute
SPA	System Performance Advancement
TGU	turbine generator unit
VFD	Variable Frequency Drive

List of Figures

List of Tables

1.0 Executive Summary

This Project investigated, analyzed and modeled advanced turbine control schemes with the objective of increasing the energy harvested by hydrokinetic turbines in turbulent flow. Ocean Renewable Power Company (ORPC) implemented and validated a feedforward controller to increase power capture; and applied and tested the controls on ORPC's RivGen® Power Systems in Igiugig, Alaska. Assessments of performance improvements were made for the RivGen® in the Igiugig environment and for ORPC's TidGen® Power System in a reference tidal environment. Annualized Energy Production (AEP) and Levelized Cost of Energy (LCOE) improvements associated with implementation of the recommended control methodology were made for the TidGen® Power System in the DOE reference tidal environment.

System Performance Advancement (SPA) goals were selected for the project. SPA targets were to improve Power to Weight Ratio (PWR) and system Availability, with the intention of reducing Levelized Cost of Electricity (LCOE). This project focused primarily reducing in PWR. Reductions in PWR of 25.5% were achieved. Reductions of 20.3% in LCOE were achieved.

This project evaluated four types of controllers which were tested in simulation, emulation, a laboratory flume, and the field. The adaptive $K\omega^2$ controller performs similarly to the non-adaptive version of the same controller and may be useful in tidal channels where the mean velocity is continually evolving.

Trends in simulation were largely verified through experiments, which also provided the opportunity to test assumptions about turbine responsiveness and control resilience to varying scales of turbulence. Laboratory experiments provided an essential stepping stone between simulation and implementation on a field-scale turbine. Experiments also demonstrated that using "energy loss" as a metric to differentiate between well-designed controllers operating at an optimal tip-speed ratio set-point is difficult, which anticipated the outcome from field experiments.

The clear message is that the feedforward $K\omega^2$ controller out-performs the feedback controllers in almost all aspects and modes of evaluation. The controllers proved a substantial improvement over the baseline performance of the TidGen® turbine, in terms of energy capture.

The effects of noise-contaminated angular velocity signals were investigated and validated by simulation as an explanation for the performance limitations observed for TidGen® turbine operations in Eastport, Maine.

Measurements of loads performed as part of the laboratory testing indicate that there are limited differences in average axial thrust force between control architectures. This suggests that none of the control strategies are likely to substantially affect loads on the turbine support structure.

Velocity measurements during the ORPC RivGen® turbine deployment at Igiugig, Alaska, in 2014 were used to assess the variability of the river flow. Results suggest that the river flow is approximately steady, in the mean sense, at any particular location in the river, with random turbulent fluctuations that are around 10% of the mean flow. The mean flow in the center channel of the river is 2.5 m/s, with reductions near the riverbanks and in the shallows. Spectral analysis and lagged correlation results indicate that temporal fluctuations at a given point are dominated by large scale fluctuations, such that measurements at the turbine location are just as useful for inflow control implementation as upstream measurements.

At this site, and likely at many other river sites, flow is generally steady at a given location, but flow varies dramatically between locations, particularly laterally across the river. The primary result is that a lateral change in position of a few meters results in changes to flow speed that far exceed the turbulence fluctuations at any given location. The turbulence is dominated by long time scales.

Following final system tests, the RivGen® device was submerged and each evaluated controller was tested across a range of gain/set point values and filter configurations for a minimum of 5 minutes, with longer runs attempted for well-performing cases.

The metric of "energy loss", the ratio of energy actually harvested by the turbine to the energy that could have been harvested by a turbine operating at maximum efficiency over a period of time was initially proposed as the sole benchmark of controller effectiveness. This metric was able to differentiate between controllers in simulation, but not in the laboratory or the field. However, for other non-ORPC turbines with higher moments of rotational inertia or performance curves with sharper roll-offs around their peak efficiency, controller choice could significantly affect power generation in turbulent flow and energy loss might be a distinguishing metric.

A systems integration analysis was performed to define an achievable, near term system architecture that would fully utilize the capabilities of the advanced control system developed within this project while integrating the parallel technologies that have been either been demonstrated in the field or are predicted by design tools that have been validated by actual deployments.

By utilizing the cost and performance models developed in collaboration with NREL for the baseline and earlier impact projections, ORPC identified specific cost and performance changes which will improve the technology.

In addition to testing controllers during the 2015 deployment season, LGL Alaska Research Associates Inc. (LGL) performed a fish monitoring study in compliance with Alaska Department of Fish and Game fisheries habitat permit for the project. During the season, LGL reviewed 10% of 179 one-hour blocks of footage (6 minutes on the hour) and documented a total of over 1200 fish in the vicinity of the RivGen® device, including over 800 salmon smolt and over 350 adult salmon. No evidence of adverse effects including passage delay by upstream migrating salmon was noted. This is an important result for future deployments and has a direct impact on commercial system designs.

The next step of development leading from this project would be to implement an adaptive $K\omega^2$ controller on a tidal turbine to verify the expected performance benefit.

2. 0 Comparison of Actual Accomplishments with Project Goals and Objectives

This Project investigated, analyzed and modeled advanced turbine control schemes with the goal of increasing the energy harvested by hydrokinetic turbines in turbulent flow.

System Performance Advancement (SPA) goals were projected for the project. SPA targets were to improve Power to Weight Ratio (PWR) and system Availability, with the intention of reduction Levelized Cost of Electricity (LCOE). This project focused primarily reducing in PWR.

Table 1: System Performance Advancement Metrics

	SPA Target	Project Achievement
Category	*% change from baseline*	*% change from baseline*
AEP (kWh)	25.0%	25.5%
PWR (kW/ton)	25.0%	25.5%

The Project objectives included the following:

1. Investigate, analyze and model advanced feedforward MHK turbine control schemes
2. Measure turbulence in situ and assess its effect on power and energy production from an operating cross-flow turbine
3. Implement and validate a feedforward controller making use of preview information from one or more single-beam transducers to increase power capture by applying it to ORPC's family of cross-flow turbine power systems
4. Refine the control scheme and provide a plan for how this control scheme will be integrated across the family of ORPC MHK devices

All Project objectives were accomplished and the overall Project goal achieved. ORPC implemented and validated a feedforward controller to increase power capture; and applied and tested the controls on ORPC's RivGen® Power Systems in Igiugig, Alaska. Assessments of performance improvements were made for the RivGen® in the Igiugig environment and for ORPC's TidGen® Power System in a reference tidal environment. Annualized Energy Production (AEP) and levelized cost of energy (LCOE) improvements associated with implementation of the recommended control methodology were made for the TidGen® Power System in the reference environment.

Table 2: Summary Comparison of Project Objectives and Achievements. All Project objectives were accomplished and the overall Project goal achieved.

Project Objective	Result	Summary
1. Investigate, analyze and model advanced feedforward MHK turbine control schemes	Accomplished	• Multiple control schemes were developed and evaluated through simulation, laboratory experiments and field operation, including $K\omega^2$ and Adaptive $K\omega^2$ nonlinear controllers, and PI-ω and PI-λ linear controllers
2. Measure turbulence in situ and assess its effect on power and energy production from an operating cross-flow turbine	Accomplished	• Thorough resource characterization was conducted to evaluate site turbulence and flow dynamics, with significant strides made in advancing the understanding of flow measurement methods, riverine turbulence and MHK device interaction with its resource.
3. Implement and validate a feedforward controller making use of preview information from one or more single-beam transducers to increase power capture by applying it to ORPC's family of cross-flow	Accomplished	• $K\omega^2$ was implemented with new power electronics architecture that reduced control system efficiency losses from 17.8% to 0%, operating stably at peak performance on the RivGen®without stall • An Adaptive $K\omega^2$ control scheme was evaluated successfully at the experimental level for

turbine power systems		application to TidGen® • SPA target metrics and achievements: ✓ Increase PWR by 25%: PWR and AEP increased by 25.5% ✓ Reduce LCOE by 20%: LCOE reduced by 20.3%
4. Refine the control scheme and provide a plan for how this control scheme will be integrated across the family of ORPC MHK devices	Accomplished	• Comprehensive assessment performed of Advanced Controls design towards system integration • New system architecture defined with near term, achievable design enhancements to optimize control system technology • Breakthrough performance gains and cost reductions predicted: ✓ Increase AEP increased by 249% ✓ Reduce LCOE by 94%

Objective 1: Model advanced feedforward MHK turbine control schemes

This project evaluated four types of controllers:

1. $K\omega^2$ – a nonlinear feedforward controller
2. Adaptive $K\omega^2$ – a nonlinear feedforward controller
3. PI-ω – a linear feedback controller
4. PI-λ – a linear feedback controller that requires preview information

These controllers were tested in simulation, emulation, a laboratory flume, and the field.

Trends in simulation were largely verified through experiments, which also provided the opportunity to test assumptions about turbine responsiveness and control resilience to varying scales of turbulence. Laboratory experiments provided an essential stepping stone between simulation and implementation on a field-scale turbine. Experiments also demonstrated that using “energy loss” as a metric to differentiate between well-designed controllers operating at an optimal tip-speed ratio set-point is difficult, which anticipated the outcome from field experiments.

The controllers were developed and tested through a combination of simulation, emulation, laboratory experiments, and field operations, as summarized in Table 3. In simulation, the turbine response to inflow conditions is deterministic and performance evaluations are rapid, enabling a low-cost exploration of parameter spaces. However, the simulated dynamics parameterize a number of aspects of turbine operation and, in combination with deterministic behavior, may not be fully representative of real systems. Emulation allows control strategies to be implemented on hardware with similar time constants to actual systems and investigate control strategies and power train responses to variations in mechanical power produced by a turbine. However, like simulation, the hydrodynamic response to turbulence and control actuation is deterministic.

Laboratory experiments allow controllers to be tested with unsteady dynamics in an environment with low-noise measurements of inflow velocity, such that turbine mechanical performance can be readily characterized. However, as for all experiments, scale disparities between the laboratory and the field can confound interpretation of results. Field operation of controllers demonstrates their true effectiveness, though uncertainty is higher than in simulation, emulation, or experiment owing to

imperfect information about inflow conditions. Further, the mechanical response of the turbine is obscured by the power train since only rotation rate and electrical power are known, rather than mechanical torque and structural loads.

Table 3: Controller development and testing summary

Controller	Simulation	Emulation [d]	Laboratory Experiments	Field Operations
PI-ω	RivGen & Lab Turbines [a,b]	RivGen Turbine	Lab Turbine [a,b,c]	RivGen Turbine VFD [b,e] & Satcon
Kω [2]	RivGen, TidGen, & Lab Turbines [a,b]	RivGen Turbine	Lab Turbine [a,b,c]	RivGen Turbine VFD [b] & Satcon
PI- λ	RivGen & Lab Turbines [a,b]	RivGen Turbine	Lab Turbine [a,b]	—
Adaptive Kω [2]	—	—	Lab Turbine	—
Measurements				
Velocity Measurement	—	—	ADV	AWAC array
Turbine Measurements	—	—	ω, τ (3-axis), and F (3-axis)	ω and P_e

Numerical turbine simulations were implemented in MATLAB Simulink with a parameter space that allowed investigation of control architectures and their performance with noise addition and filtering. The controller produces a command torque signal based on an estimate for the rotation rate and, in the case of PI-λ control, an estimate for the free stream velocity. This control torque and actual free stream velocity act on the turbine, changing its rotation rate. The simulation integrates the turbine dynamic equation forward in time using a variable-step integrator. Uncertainty in the rotation rate passed to the controller is simulated by a logic block that can add noise to the actual rotation rate (representing an inaccuracy in the controller's inherent estimate for rotation) and attempt to improve the estimate through filtering.

The simulation was adapted to accommodate RivGen®, TidGen®, and the flume turbines. In simulation, inflow time series for each turbine were obtained from ADV measurements, filtered by a cut-off frequency defined by the turbine bandwidth (i.e., the frequencies of motion to which the turbine power generation is sensitive).

Laboratory experiments were carried out at the Marine Sciences Centre in Bamfield, BC, Canada. The primary objective of the experiments is to explore simulated control architectures on an actual turbine, and use the results to design controllers for a full-scale turbine. For results to scale accurately between turbines, their dynamic response to controls inputs and turbulent perturbations must be similar.

Electromechanical emulation machines (EEMs) have been shown capable of mimicking the dynamic performance of a hydrokinetic turbine in a laboratory environment and allow the development of a PTO and control strategy prior to field deployment (Cavagnaro et al., 2015). An EEM at the MaREI-HMRC test center at University College Cork, Ireland was utilized to emulate the RivGen® turbine and evaluate several aspects of PTO integration and control.

The effects of noise-contaminated angular velocity signals were investigated as an explanation for the performance limitations observed for TidGen® turbine operations in Eastport, Maine. The TidGen® $K\omega^2$ controller updated at a rate of 2000 Hz, substantially faster than the highest energy-containing frequencies of turbulence in tidal channels (Thomson et al. 2012).

Controller performance from simulation predictions, laboratory testing and emulation are presented below.

Table 4: Simulated energy loss for RivGen®, TidGen®, and flume turbines under PI-ω, PI-λ, and $K\omega^2$ controllers with added noise (N) and filters (F+N).

	PI-ω			$K\omega^2$			PI-λ		
Turbine	**Base**	**N**	**F+N**	**Base**	**N**	**F+N**	**Base**	**N**	**F+N**
RivGen	3.9	20.3	20.3	2.6	16.0	5.9	3.6	14.5	14.6
TidGen	4.1	28.3	28.3	0.8	34.1	4.8	1.6	32.0	32.1
Flume	25.4	25.9	25.5	25.3	25.9	25.5	25.4	26.0	26.0

Table 5: E_{loss} [%] for laboratory experiments

Controller	Baseline	Added Noise	Added Noise and Filtering
PI-ω	5	7	-2
$K\omega^2$	2	3	0
PI-λ	4	3	3

Table 6: E_{loss} [%] for performance of controllers in emulation

Controller	E_{loss} [%] - mechanical	E_{loss} [%] - electrical
PI-ω	2.2	5.3
$K\omega^2$	0.5	4.4
PI-λ	1.5	6.7

Measurements of loads performed as part of the laboratory testing indicate that there are limited differences in average thrust force between control architectures. This suggests that none of the control strategies are likely to substantially affect loads on the turbine support structure.

Emulation of controllers on hardware at University College Cork provided early validation of simulation results for minimum update rates and successfully reproduced the performance of the RivGen® turbine during 2014 field trials. Field testing confirmed trends identified in simulation, emulation, and experiments, but success in the field campaign would not have been likely without these other investigations.

Objective 2: River Measurements

Two separate deployments of the RivGen® Power System were conducted in the Kvichak River in Igiugig, Alaska. In 2014 the system was deployed and velocity measurements were made by researchers from the University of Washington to assess the variability of the river flow. Performance of the system was

characterized. In 2015, the system was again deployed and control schemes implemented and tested. As part of the 2015 work, the river resource was again mapped and measured.

Velocity measurements during the Ocean Renewable Power Company's RivGen® turbine deployment at Igiugig, Alaska, in 2014 were used to assess the variability of the river flow. The first objective was to understand the spatial variability of the inflow velocities for RivGen®, in particular the strong spanwise shear that occurred at the RivGen® location. The second objective was to understand the time variability of inflow velocities, in particular the streamwise coherence of the inflow velocities. Results suggest that the river flow is approximately steady, in the mean sense, at any particular location in the river, with random turbulent fluctuations that are around 10% of the mean flow. The mean flow in the center channel of the river is 2.5 m/s, with reductions near the riverbanks and in the shallows. As the flow is quasi-steady, the data from various stations can be gridded to a synoptic flow map around the turbine, showing strong inflow velocity gradients across the turbine.

Spectral analysis and lagged correlation results indicate that temporal fluctuations at a given point are dominated by large scale fluctuations (> 10 s), such that measurements at the turbine location are just as useful for inflow control implementation as upstream measurements. The turbulence spectrum is equivalent to the lagged auto-correlation of a given velocity time series. The correlation between two simultaneous independent measurements shows almost an identical result. This is contrary to the expectation of a distinct, sign-definite lag between the two measurements, as would be expected if the flow was truly a frozen signal advecting along or was wave-like. Such a flow would be the ideal case for implementing feed-forward control in a turbine, because an upstream measurement could be projected to the turbine with a known time lag.

Despite the general lack of coherent lags in simultaneous flow measurements at various separation distances, the inflow at the site RivGen® is still amenable to control strategies. The streamwise flow appears to be coherent at large space and time scales. On short space and time scales (i.e., small eddies), the turbulence likely evolves too quickly to observe lags, and on longer time scales the lags are essentially zero for separations of order ~ 10m. The zero lag result dominates because the longer scales contain the most energy. Thus, at any individual fixed point, such as the turbine location, the most robust preview of the flow would be the previous 10 to 30 s of flow *at that location*. An upstream measurement would have no increased skill relative to this self-forecast, because the only thing different at the upstream measurement location would be the small, incoherent eddies. Restated: the large velocity fluctuations tend to last at least 10 s, and on those time scales localized measurements are equivalent to any upstream measurement.

At this site, and likely at many other river sites, flow is generally steady at a given location, but flow varies dramatically between locations, particularly across the river. The primary result is that a lateral change in position of a few meters results in changes to flow speed that far exceed the turbulence fluctuations at any given location. The turbulence is dominated by long time scales.

Objective 3: Implement and validate a feedforward controller

The RivGen® Power System consists of a turbine generator unit (TGU) that rests on a pontoon structure that in turn sits directly on the river bed when submerged. The 2015 version of the system has increased pontoon lengths to increase hull speed and to provide additional buoyancy to assist with system towing, deployment and retrieval; and a fairing added to the chassis to increase turbine capture area. The RivGen® Power System has the same operating principles and design characteristics as the TidGen® turbine but is intended for deployment in shallow river sites only, due to its smaller cross sectional area, and pontoon support structure.

Following final system tests, the RivGen® device was submerged. Despite operational challenges, the deployment of the RivGen® device to the river bottom went well and proved to be a controlled process consistent with model predictions.

In 2015 the shore station was capable of operating the RivGen® turbine through two different rectifiers, two different inverters, and supplying power to two different loads. Because of grid connection difficulties in 2014, it was deemed prudent to have several different means of grid connection on site, with the major point of redundancy being the availability of a SMA 20kW PV inverter and a Satcon PowerGate 50kW PV inverter. Both inverters were tested during prior dynamometer tests with a simulated diesel micro grid, and both were functional with the RivGen® generator, although the Satcon inverter was limited with a narrow voltage range, and the SMA inverter was unable to accept external controller commands. Due to these limitations, an ABB ACS880 variable frequency drive (VFD) was incorporated into the architecture to control the generator output at the rectification stage using the desired control schemes. In addition to the inverters, the system featured a secondary DC load bank capable of dissipating power from the RivGen® TGU through a DC load bank that enabled control and testing of the RivGen® without exporting power to the Igiugig grid.

To quantify temporal-spatial variations in the shear profile, two upstream-looking 2-beam Nortek AWAC 400 kHz Doppler sonars were mounted at each end of rotor. The beams were separated by 50^{o} in look-angle, the velocities were sampled at 1 Hz, and the Doppler noise was 0.05 m/s. The AWACs are vertically offset by 1 m to limit cross-talk at the horizontal intersection of the beams.

Once an estimate of the representative inflow velocity has been obtained, turbine performance can be estimated. The RivGen® turbine performance was characterized by stepping the turbine through a series of load settings imposed by resistance elements on the shore station, and by use of constant voltage mode with the SMA inverter. The inflow velocity and, therefore, hydrodynamic torque is approximately constant over this period, so the turbine tip-speed ratio (λ) is as well. There is a 35% improvement over the 2014 performance curve, which is explained by the addition of a fairing to the RivGen TGU for the 2015 testing.

This project evaluated four types of controllers in field testing utilizing the VFD:

1. $K\omega^2$ – a nonlinear feedforward controller
2. PI-ω – a linear feedback controller
3. PI-λ – a linear feedback controller that requires preview information
4. A constant omega control native to the VFD

Each evaluated controller was tested across a range of gain/set point values and filter configurations for a minimum of 5 minutes, with longer runs attempted for well-performing cases. A SCADA-controlled PI-TSR controller was tested but proved impossible to operate in a stable fashion, likely due to noise and data drop outs in inflow measurements from AWAC measurements.

The performance of each controller and filter strategy was considered in terms of the range of tip-speed ratios at which it could operate stably, variability of command torque and power output, and ability to hold a set point. Energy loss calculations, used to differentiate controllers in simulation and emulation, do not show significant differences between different control strategies in the field, as shown in Table 25. There are two reasons for this. Controllers are able to operate stably at the optimal tip-speed ratio and the performance curve changes slowly about this point. Therefore, undershoot and overshoot for the feedback controller has limited effect on power generated.

Outcomes from testing modalities are summarized in Table 7. The clear message is that the feedforward $K\omega^2$ controller out-performs the feedback controllers in almost all aspects and modes of evaluation. The conclusions drawn from single modalities of testing are generally shared. In practice, the energy capture differences between controllers (while a substantial improvement over the baseline performance of the TidGen® turbine) were minimal in the laboratory and field. Each testing modality also contributed unique information about controller performance, measurement, and implementation.

The metric of “energy loss”, the ratio of energy actually harvested by the turbine to the energy that could have been harvested by a turbine operating at maximum efficiency over a period of time was initially proposed a the sole benchmark of controller effectiveness. This metric was able to differentiate between controllers in simulation, but not in the laboratory or the field. However, for turbines with higher moments of rotational inertia or performance curves with sharper roll-offs around their peak efficiency, controller choice could significantly affect power generation in turbulent flow and energy loss might be a distinguishing metric.

During the 2015 deployment season LGL Alaska Research Associates Inc. (LGL) performed a fish monitoring study in compliance with and Alaska Department of Fish and Game fisheries habitat permit for the project. The study collected data from 5 video cameras mounted on the RivGen® device. LGL collected video data for a total of 415 hours, 240 hours during which the RivGen® was in operation. Continuous video footage was collected through the last week of July during the latter half of the peak of the adult sockeye salmon migration. During this time 1.5 million sockeye salmon migrated upstream past the turbine. After this time period 50% video coverage of RivGen® operations was maintained. During the season LGL reviewed 10% of 179 one-hour blocks of footage (6 minutes on the hour) and documented a total of over 1200 fish in the vicinity of the RivGen® device, including over 800 salmon smolt and over 350 adult salmon. No evidence of adverse effects including passage delay by upstream migrating salmon was noted.

Over the course of the 2015 operations the RivGen® Power System logged a total of 382 hours of operations producing over 2 MWh of power delivered to the Igiugig grid.

Table 7: Testing modality outcomes

Outcome	Simulation	Emulation	Laboratory Flume	Field
Energy Capture (E_{loss})	$K\omega^2$ superior (smallest E_{loss})	PI-ω superior (smallest E_{loss})	Minimal difference	Minimal difference
Stability at $\lambda < \lambda^*$	$K\omega^2$ superior (most stable)	-	$K\omega^2$ superior (most stable)	$K\omega^2$ superior (most stable)
Range of Command Torque	$K\omega^2$ superior (smallest range)	-	$K\omega^2$ superior (smallest range)	$K\omega^2$ superior (smallest range)
Range of ω	PI- ω superior (smallest range)	-	PI-ω superior (smallest range)	PI-ω superior (smallest range)
Minimum Update Rate	10 Hz	10 Hz	-	-
Impact of Sensor Noise	Degrades stability	-	Degrades stability	-
Effect of Filtering	Recovers stability	-	Recovers stability	Reduces stability[1]
Unique Insights		Emulation achieves good agreement with field observations	Controller performance unaffected by increased turbulence	- Observations of turbine wake - Potential for large improvement through blockage - New capability to characterize turbines in sheared flow

Objective 4: System integration plan

During testing in Cobscook Bay, Maine, the TidGen® turbine generator was actuated by a non-linear $K\omega^2$ controller. The system could not, however, operate stably with $K = K^*$, which reduced the maximum operational efficiency to 80% of peak, even with an update rate of 2000 Hz. The most consistent explanation for this performance limitation is a noisy estimate for the rotation rate being used to calculate the control torque. This could either be addressed through filtering or modifications to bring the calculation of rotation rate more in line with the method used by the Variable Frequency Drive (VFD) in RivGen® 2015 turbine testing. Based on the results of this project, the latter would yield better performance.

In a tidal environment, the mean currents will change continually from slack to peak flow. Initially, to maximize power, an adaptive $K\omega^2$ controller might need to be employed if the turbine's efficiency is a function of both velocity and tip-speed ratio. All test work show that a properly tuned adaptive $K\omega^2$ controller can maintain optimal efficiency for a time-varying inflow velocity. Beyond the turbine's rated speed, the control objective would shift from maximum efficiency to maintaining a constant power output. The $K\omega^2$ controller can be used to achieve this by adjusting K to a value away from K^*. This is another form of an adaptive $K\omega^2$ controller.

Despite the invariance of the plant model found in the Kvichak River, a secondary effect related to the site characteristics appears to be important. Following initial tow testing and TGU characterization in Eastport, ME in 2014, a given system efficiency was expected for the RivGen. However, when the system

[1] This is reduction in stability is hypothesized to have more to do with the specific filter implementation on hardware than an inherent stability reduction through filtering for a given class of controller.

was deployed in Igiugig in a shallow river, the performance of the system significantly increased. Explanations for this shift in behavior have been proposed to be either the effects of blockage or the presence of a free surface as an upper boundary condition. Based on CFD modeling we hypothesize that increases in power coefficient are directly related to the increases in the flow through the turbine which in turn increases the drag forces experienced by the system. Since the plant model depends on absolute performance of the system, this implies that a characterization exercise for each turbine at each site is required to obtain the optimal control parameters.

A secondary goal of the project was to assess the effects of controllers on system loads, with the intention of actively reducing load if possible. During laboratory testing thrust loads were measured on the system for different controller modes and operating conditions. There are limited differences in average axial thrust force between control architectures, including with noise addition and filtering. This suggests that none of the control strategies are likely to substantially affect loads on the turbine support structure. The trend of increasing thrust loads for the $K\omega^2$ and PI-ω controllers away from the optimal tip speed ratio ($\lambda \sim 1.3$) are notable and may be of interest for future investigation.

Because of the findings of the field testing in 2015, it can be concluded that future commercial projects will not require real time water velocity measurements, assuming the site and turbines are properly characterized, or a standalone rotation rate measurement, assuming a native measurement is taken by the rectifier.

Conclusions and Lessons Learned

At project initiation, the state-of-the-art in the wind industry indicated that an optimal controller for a cross-flow hydrokinetic turbine would require preview information about the flow field, likely assimilated into Model Predictive Control. The conclusion of this project is that for cross-flow turbines with a high aspect ratio (i.e., low rotational inertia) in a riverine environment, a simple, non-linear feedforward controller (control torque prescribed by $K\omega^2$) can effectively harness all useful turbulent kinetic energy from a flow. This controller also minimizes the range of command torque signals required to hold a desired set-point. For this type of turbine, the only way to significantly further increase energy yield is by increasing the fundamental performance coefficient for a given operating condition.

While simulation was proposed from the start of the project as the sole tool for developing field-scale controllers, emulation and laboratory experiments proved valuable in developing robust control algorithms. Future control investigations would benefit from a similar diversity of methods. Fundamental to the development and evaluation of an optimal controller is information about the performance characteristics of a turbine. The emphasis placed by this project on characterizing inflow conditions provided a number of unexpected insights into turbine-resource interactions. Specifically, in riverine environments, power enhancement from confined flow was much more substantial than anticipated from prior knowledge and still not fully understood. If better understood, this effect could be used to significantly increase the technically recoverable river current resource. Second, the presence of strong lateral shear required the development of a new approach for estimating the inflow velocity needed to non-dimensionalize turbine performance. This method, developed through this project, has been incorporated into a technical specification for river current turbine performance being developed through international standards committees.

The next step of development leading from this project would be to implement an adaptive $K\omega^2$ controller on a tidal turbine to verify the expected performance benefit.

3.0 Summary of Project Activities

3.2 Project Planning

3.2.1 Original Hypotheses

A Project Management Plan (PMP) was to be developed, finalizing the Project objectives, deliverables, schedules, Gantt charts, technical risk mitigations, risk management procedures, funding and costing profiles, work breakdown structures, project organization and structure.

ORPC and partners would finalize the draft intellectual property management plan (IPM). The finalized plan was to serve as the coordinating document between Project partners and addressing issues related to control and dissemination of confidential information, intellectual property and data, and the handling of commercialization arrangements, as well as providing means and methods for resolving intellectual property disputes between partners.

3.2.2 Approaches Used

The Project Management Plan was developed as planned with input from the project team. The plan provided a means for controlling the project schedules and budgets.

The intellectual Property Management Plan was completed and signed by team members on January 21, 2014. The Principal Investigators have strong track record of successful collaboration on joint projects including work pursued under DOE funding. Intellectual property, both existing and that developed pursuant to the Project, was managed consistent with the Intellectual Property Management Plan.

3.2.3 Problems Encountered and Departure from Planned Methodology

No issues of significance arose during negotiation of either the PMP or the IP. All team members directly funded by ORPC accepted and worked well within the project management structure. All team members accepted and work to the IP management plan.

3.2.4 Assessment of Their Impact on the Project Results

The plans added a level of control and transparency to the project which improved project management and control. The project was completed on time and within budget for all team members.

The IP management plan clarified means and methods of publication for team members. Multiple papers and presentations were made related to the project. Intellectual property concerns related to the publication of these results were not an issue.

3.3 Development and Simulation of Control Algorithms

3.3.1 Original Hypotheses

Under Task of the Project, ORPC and partners would develop a control algorithm for RivGen® and TidGen® TGUs able to make use of preview information about the evolving velocity field to preemptively adjust generator torque to better track energy-containing eddies. This would make use of resolved turbulent inflow measurements.

Preview information was to be targeted to be collected from a range of between 50 to 100m upstream of the turbine, on a time scale of seconds to minutes. Turbulence measurements were to be made with

different instruments, signal to noise ratios assessed, and various metrics of turbulence will be evaluated to define candidate control signals.

ORPC and partners would develop a numerical model of the ORPC TGUs. Initially, this was to be used to simulate and refine the existing feedback controller, but would, ultimately include hybrid feedback-feedforward control with preview information about the velocity field. The feedback and feedforward control models were to be validated against RivGen® Power System performance data.

Originally validation of the control schemes was proposed as part of Task 4 of the project. In the interests of providing a clearer narrative work related to the validation of controls schemes by simulation, laboratory testing, and emulation are presented here. The original hypothesis for this portion of the work is outlined below.

Provided that the Task 4.1 stage gate is satisfied, feedforward control will be implemented on an ORPC TGU. This will likely require additional Doppler instrumentation to be installed on the TGU and the optimal feedforward controller (Task 2.0) implemented in hardware on either the TGU or shore control station.

Design of the controller will involve the following:

- Selection of appropriate low pass filter cutoff frequency for velocity and rotational rate measurements
- Determination of appropriate sample rate for controller inputs
- Investigation of filer and sampling rates on system noise characteristics

The selection of appropriate parameters will be informed, to the extent possible, by controller simulation, laboratory experiments with candidate controllers on a scale-model turbine, and CFD modeling. As part of this task, a test matrix for laboratory experiments and CFD modeling will be developed.

3.3.2 Approaches Used

3.3.2.1 Background

Performance of a hydrokinetic turbine can be considered as a combination of water to wire efficiency and stability of operation. The maximum energy production from a system is achieved when the system operates stably and sustainably at its peak efficiency. The water-to-wire efficiency (η) of a hydrokinetic turbine varies as a function of tip-speed ratio (λ). The efficiency relates the electrical power produced by the turbine to the kinetic energy flux through its swept area. This is given as

$$\eta = \frac{P_{\text{electrical}}}{\frac{1}{2}\rho U^3 A} = \frac{P_{\text{mechanical}}\ \eta_{\text{powertrain}}}{\frac{1}{2}\rho U^3 A} = C_P \eta_{\text{powertrain}}$$

where $P_{\text{electrical}}$ is the electrical power generated by the turbine (the product of mechanical power extracted by the turbine rotor and mechanical and electrical power train efficiencies) and the terms in the denominator (density, ρ; free stream velocity, U; and rotor swept area, A) describe the kinetic energy flux through the rotor swept area. The coefficient of performance (C_P) is a measure of the

efficiency with which the turbine converts kinetic power to mechanical power. The tip-speed ratio describes the speed at which the turbine blade tips rotate relative to the free stream velocity as

$$\lambda = \frac{R\omega}{U},$$

where R is the turbine radius and ω is the rotation rate.

The primary objective of a control system is to allow the turbine to operate stably at a desired set-point along its performance curve in response to time-varying inflow conditions and variable load conditions. Secondary objectives can include minimizing structural loads.

The evolution of the turbine rotation rate in time can be described by

$$\frac{d\omega}{dt} = \frac{1}{J}\left(\tau_h - \tau_c - B\omega\right),$$

where J is the rotational moment of inertia of the turbine (included added mass), τ_h is the hydrodynamic torque produced by the rotor, τ_c is the torque applied by the generator, and B parameterizes the damping in the system. Torque applied by the generator is the control torque.

Cross-flow turbines differ fundamentally from horizontal axis turbines in that their axis of rotation is perpendicular to the inflow. In general, cross-flow turbines do not have the ability to adjust the pitch of their blades to control hydrodynamic torque and rely on adjustment of the generator control torque to regulate turbine speed. Typical implementations of torque control for cross-flow turbines are adapted from the wind industry (Pao & Johnson 2011). There is limited literature on cross-flow specific controller development, and almost none specifically dealing with hydrokinetic cross-flow turbines (Ginter & Pieper 2011). As a result, these schemes may need to be modified to account for issues specific to cross-flow hydrokinetic turbines, such as their sensitivity to turbulence and, for large aspect ratios, the possibility of a strongly sheared inflow.

The state of the art in wind turbine control systems research is “preview” methods that can apply a control torque in advance of a disturbance that will affect a turbine. For example, Model Predictive Control (MPC) forecasts the response of a system to future disturbances in a way that maintains the system at a desired set-point. All preview controls require a model for the system performance and an accurate estimate of future disturbances over some time horizon. Given this, the project team initially expected that improving the performance of cross-flow hydrokinetic turbines would require similar methods – developing a preview controller that allowed the turbine to anticipate disturbances in the flow and take action to avoid set-point undershoot or overshoot.

However, this proved not to be the case for two reasons. First, the moment of inertia varies with the square of the distance between a mass (turbine, generator) and the axis of rotation. If an axial-flow and cross-flow turbine has the same swept area and solidity, a cross-flow turbine with a high aspect ratio will often have a lower moment of inertia as more of its mass is closer to its axis of rotation. Consequently, some cross-flow turbines are able to react quickly to flow disturbances. In the case of the specific turbines considered as part of this project, this response was fast enough to obviate any benefit from preview control, given the inherent uncertainties in the estimate for inflow velocity. Second, measurements in the field demonstrated that the turbine power is primarily affected by large-scale turbulence that acts coherently across the entire rotor. In riverine environments, estimates of this turbulence can be obscured by strong spatial gradients in the flow, such that a fluctuation measured

upstream cannot be used for a preview at a downstream location. In tidal environments, this might not be the case, but a cross-flow turbine with low rotational inertia would still see limited benefit from preview information.

3.3.2.2 TidGen® and RivGen® Power Systems

ORPC's TidGen® turbine project, the Cobscook Bay Tidal Energy Project, deployed a 150 kW rated TidGen® turbine off the coast of Eastport and Lubec, Maine, in 2012. This TidGen® TGU operated over 8 months sending power to the local grid.

The means of controlling the output of the TidGen® generator was by modifying the duty cycle of the Pulse Width Modulation (PWM) of the AC to DC converter in the subsea converter module. For the TidGen® turbine a torque control algorithm was implemented with torque settings determined by

$$\tau_c = A\omega^3 + B\omega^2 + C\omega + D$$

where τ_c is the control torque applied (N-m), ω is the turbine rotation rate (rpm), and *A*, *B*, *C*, and *D* are user-specified constants. For the most reliable performance of the TidGen turbine, parameters *A*, *C*, and *D* were set to zero, such that the control torque was proportional to the square of the rotation rate (an implementation of $K\omega^2$ control).

An issue was encountered with this setup in that instability in the generator output caused the turbines to stall at points near peak performance. In reality, the maximum sustainable turbine efficiency for the TidGen® Power System was 19% lower than the actual maximum.

As discussed in this report, it is hypothesized that the inability to operate at peak performance was caused by an inaccurate estimate for rotation rate used by the controller algorithm. This could have been caused by high levels of noise associated with a sampling rate orders of magnitude faster than that of the rotational frequency of the turbine. An inaccurate controller input would mean that the value of the rotation rate used to set the control torque would not correspond to the actual rotation rate.

The baseline control system for the TidGen® and RivGen® Power Systems are identical.

3.3.2.3 River environment

After measurements of turbulence performed in field in 2014 indicated that preview control would be of limited value for low inertia turbines, the project team focused on developing and testing two types of controllers: feedback and feedforward controls. A feedback controller is one that compares the present operation of a system to a desired set-point and makes control actuations to minimize the error between the two. Such a controller has no inherent knowledge of the plant response to this actuation. In contrast, a feedforward controller incorporates knowledge about the plant to provide control actuation that meets a specific objective. The optimal gain for a feedforward controller is based on a known plant response (i.e., a performance curve). Unlike a preview controller, a feedforward controller has no foreknowledge about future disturbances, but if the plant responds to control actuations as fast as it is affected by disturbances, preview information provides no benefit.

The turbulent kinetic energy spectra and generator power spectra (following frequency analysis from Thomson et al. 2012) measured during the RivGen® deployment in Iguigig, Alaska (Figure 1)shows that there is limited energy in the turbine power output at frequencies faster than 0.2 Hz, which is unsurprising, given that there is limited energy in the turbulent inflow above 0.15 Hz. Controller update

rate should be at least an order of magnitude faster than the perturbations to the system for stable performance. Therefore, a minimum update rate of 10 Hz was recommended for field testing in 2015.

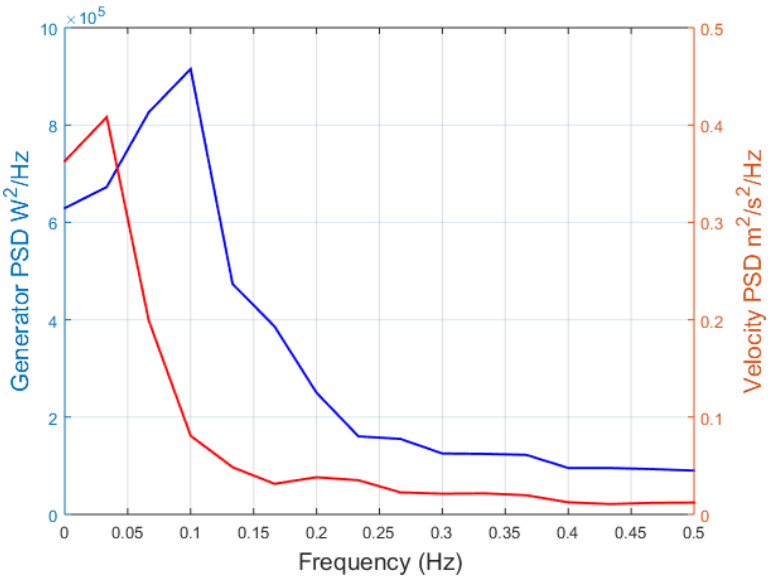

Figure 1: The free-stream velocity and generator power spectra for the RivGen turbine in Igiugig (2014 measurements). The velocity data are acquired at 16 Hz, while the generator power data is logged at 1 Hz, resulting in a broader bandwidth for the electrical power spectra.

3.3.2.4 Controllers

Three broad categories of controllers were evaluated: feedback, feedforward, and preview.

- Controller 1: *Nonlinear Feedforward* ($K\omega^2$) – This was the controller used on the TidGen® turbine and is used for maximum power point tracking in the wind industry (Pao and Johnson, 2011).
- Controller 2: *Feedback Speed Control* (PI-ω) – Linear feedback controls have well-characterized responses to disturbances and performance can be evaluated through linearization of the governing dynamics. Since the root cause of the controller issues with the TidGen® turbine was unknown at project initiation, a simple linear feedback controller was chosen as a baseline to evaluate stability.
- Controller 3: *Feedback Tip-Speed Control* (PI-λ) – Because turbine performance is a function of the tip-speed ratio, a linear feedback controller tracking this quantify will theoretically outperform one tracking rotational speed. This does, however, require an estimate for the inflow velocity.
- Controller 4: *Adaptive Nonlinear Feedforward* (Adaptive $K\omega^2$) – For real turbine systems, performance can be a function of both tip-speed and velocity. This can have several root causes, for example, a convolution of mechanical efficiency (function of λ) and non-constant power train efficiency (function of τ_c and ω). In this case, preview information can be used to adjust the nonlinear controller gain.

While Proportional plus Integral and Derivative (PID) control was also considered, PID feedback controllers often provide only a marginal benefit over PI controllers and are more susceptible to degradation from sensor noise (the derivative amplifies noise). Given that sensor noise was suspected as

a root cause for the TidGen® turbine's performance challenges, no PID feedback controllers were investigated.

3.3.2.5 Feedback speed control (PI-ω)

A linear error controller, Proportional plus Integral (PI) control, was investigated with the goal of maintaining turbine operation at a rotation rate set-point (ω^*). Control torque is the sum of a proportional gain (K_P) on speed error and an integral gain (K_I) on the integral of speed error over the total time of controller action (t),

$$\tau_c = K_P(\omega - \omega^*) + K_I \int_0^t (\omega - \omega^*) d\tau$$

where τ is the length of a numerical time step. Gains are tuned to achieve desired performance characteristics such as under/overshoot percentage, rise time, and steady-state error. The performance of this controller is therefore dependent on the selected gains, as well as update rate and quality of the measurement of ω. The controller is shown schematically in Figure 2. This discrete controller adjusts the command torque (τ_c) after a specific period of time, the inverse of which is termed the "update rate".

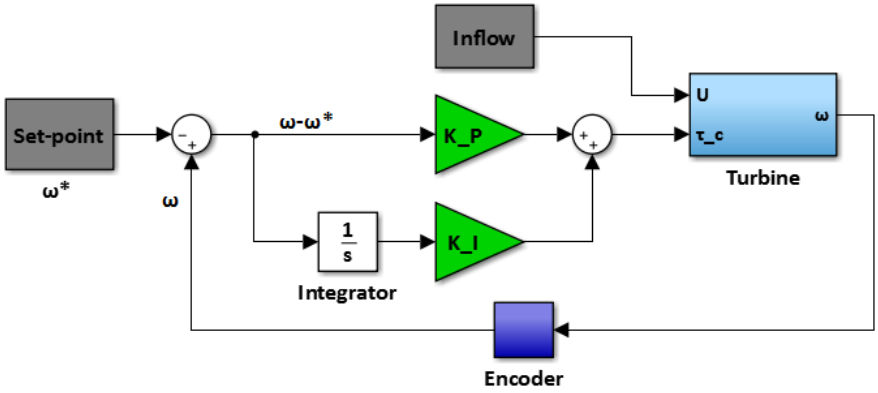

Figure 2: PI-ω controller schematic. An error signal between the desired speed setting and the reported value is used to drive the control response.

3.3.2.6 Feedback tip-speed control (PI-λ)

Similar to PI-ω control, PI-λ attempts to maintain a desired tip-speed ratio (λ^*) as defined in (2) Control torque becomes,

$$\tau_c = K_P(\lambda - \lambda^*) + K_I \int_0^t (\lambda - \lambda^*) d\tau \,.$$

PI-λ relies on a measurement of free stream velocity and its performance depends on the quality of this measurement in addition to the considerations for the PI-ω controller. However, this controller is capable of tracking the instantaneous maximum power point as defined by a turbine's performance curve. This controller is shown schematically in Figure 3.

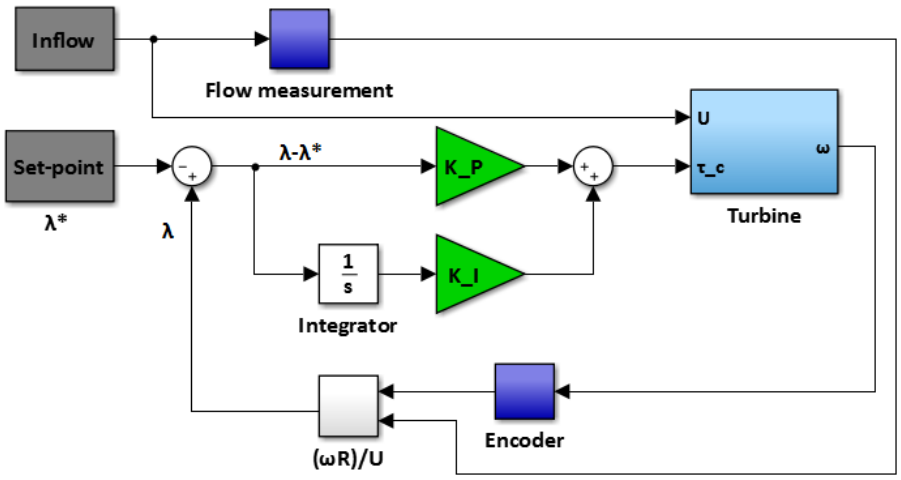

Figure 3: PI-λ controller schematic. Measured tip speed ratio is compared to the desired set-point to generate an error signal which is corrected by the controller.

3.3.2.7 Nonlinear feedforward (Kω²)

Derived from the dynamic model of turbine operation, the nonlinear feedforward Kω² controller commands a torque,

$$\tau_c = K\omega^2 = \frac{1}{2}\rho A R^3 \frac{\eta(\lambda)}{\lambda^3}\omega^2$$

which brings the turbine to a desired operating point on its performance curve ($\eta(\lambda)$). In the case where K results in the turbine operating at peak efficiency, this optimal gain is referred to in this report as K^*. K values larger or smaller in magnitude than K^* result in operation to the "left" or "right" of the peak (slower or faster than optimal λ, respectively). Optimal performance requires a well-defined performance curve and accurate measurement of ω. Note that unlike a feedback controller, the control torque equation does not explicitly prescribe a fixed set-point. Rather it controls the turbine to a set-point based on the estimate for the plant dynamics. This controller is shown schematically in Figure 4.

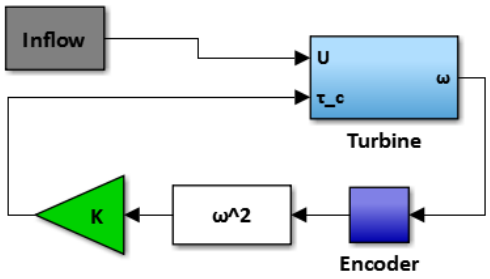

Figure 4: Kω² controller schematic. This feedforward controller creates a torque command based on the speed of the turbine and the plant characteristic K.

3.3.2.8 Adaptive nonlinear feedforward (adaptive Kω²)

An adaptive version of Kω² control can be used when a turbine's performance curve is subject to parameter variation (e.g., efficiency is a function of both tip-speed ratio and free-stream velocity). A model of this variation with free stream velocity is employed so that

$$\tau_c = K(U)\omega^2 = \frac{1}{2}\rho A R^3 \frac{\eta(U,\lambda)}{\lambda^3}\omega^2,$$

in which controller action depends on measurement of *U*. As variation in free stream velocity is considered an uncontrollable disturbance to a system, utilizing this measurement constitutes the use of 'preview' information. As with the standard formulation for this controller, its performance depends on the quality of turbine performance space and the quality of the flow speed measurement. The controller is shown schematically in Figure 5.

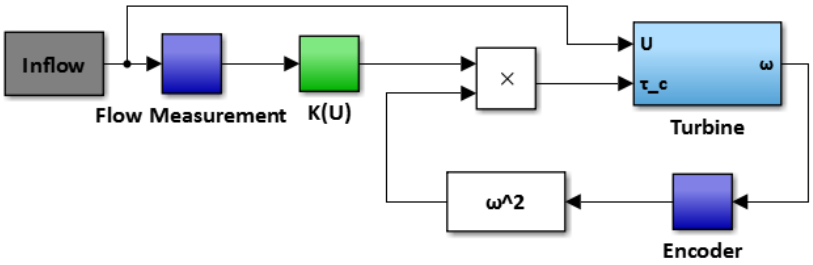

Figure 5: Adaptive Kω^2 controller schematic. The plant characteristic value, K, can be adapted for a specific value of U, or any other desired parameter.

3.3.2.9 Controller metrics

By integrating instantaneous power over time, total energy generation can be determined and compared to the energy generation by a turbine operating at maximum efficiency for this entire period. The more effective a controller, the closer it will perform to an ideal system, which can be expressed by an energy loss metric (E_{loss}):

$$E_{loss} = 1 - \frac{\int_0^t \tau_c(t)\omega(t)dt}{\int_0^t \frac{1}{2}\rho A U_\infty(t)^3 \eta_{\max} dt}$$

where $\eta_{\max}$ is the maximum turbine efficiency. As E_{loss} goes to zero, the controller is allowing the turbine to harness the maximum possible kinetic energy flux from the flow. In simulation, the free-stream velocity, torque, angular velocity, and turbine performance curve are known with perfect accuracy and any difference in E_{loss} is a significant differentiator. In experiment and field trials, where uncertainty in the calculation of E_{loss} is substantial, this can only be used to differentiate controllers with large differences in performance.

Because of this, a second measure of controller effectiveness was considered. Specifically, at a turbine-specific tip-speed ratio slower than optimal, stall will occur and rotation will cease. For a controller intended to operate the turbine at the optimal tip-speed ratio, this can occur from set-point undershoot, either inherent to the controller or exacerbated by noise in the controller inputs. For Kω^2 control, this can be expressed as a "gain ratio", defined as the ratio of *K* with stable performance (i.e., maximum *K* that does not cause turbine stall during operation) to *K**, the gain required to operate at the point of maximum efficiency.

3.3.2.10 Controller evaluation techniques

The controllers described in Section 3.3.2.4 were developed and tested through a combination of simulation, emulation, laboratory experiments, and field operations, as summarized in Table 10. In simulation, the turbine response to inflow conditions is deterministic and performance evaluations are rapid, enabling a low-cost exploration of parameter spaces. However, the simulated dynamics parameterize a number of aspects of turbine operation and, in combination with deterministic behavior, may not be fully representative of real systems. Emulation allows control strategies to be implemented on hardware with similar time constants to actual systems and investigate control strategies and power

train responses to variations in mechanical power produced by a turbine. However, like simulation, the hydrodynamic response to turbulence and control actuation is deterministic. Laboratory experiments allow controllers to be tested with unsteady dynamics in an environment with low-noise measurements of inflow velocity, such that turbine mechanical performance can be readily characterized. However, as for all experiments, scale disparities between the laboratory and the field can confound interpretation of results. Field operation of controllers demonstrates their true effectiveness, though uncertainty is higher than in simulation, emulation, or experiment owing to imperfect information about inflow conditions. Further, the mechanical response of the turbine is obscured by the power train since only rotation rate and electrical power are known, rather than mechanical torque and structural loads.

Table 8: Controller development and testing summary

Controller	Simulation	Emulation [d]	Laboratory Experiments	Field Operations
PI-ω	RivGen & Lab Turbines [a,b]	RivGen Turbine	Lab Turbine [a,b,c]	RivGen Turbine VFD [b,e] & Satcon
Kω [2]	RivGen, TidGen, & Lab Turbines [a,b]	RivGen Turbine	Lab Turbine [a,b,c]	RivGen Turbine VFD [b] & Satcon
PI- λ	RivGen & Lab Turbines [a,b]	RivGen Turbine	Lab Turbine [a,b]	—
Adaptive Kω [2]	—	—	Lab Turbine	—
Measurements				
Velocity Measurement	—	—	ADV	AWAC array
Turbine Measurements	—	—	ω, τ (3-axis), and F (3-axis)	ω and P_e

[a] testing effect of sensor noise
[b] testing effect of filters on inputs
[c] testing effect of elevated turbulence
[d] using estimates of RivGen® turbine performance from 2014
[e] implemented through VFD programming and native VFD speed control

3.3.2.11 Simulation of turbine systems

Numerical turbine simulations were implemented in MATLAB Simulink with a parameter space that allowed investigation of control architectures and their performance with noise addition and filtering. The overall simulation architecture is shown in Figure 6. The controller produces a command torque signal based on an estimate for the rotation rate (ω) and, in the case of PI-λ control, an estimate for the free stream velocity (U). This control torque and actual free stream velocity act on the turbine, changing its rotation rate. The simulation integrates the turbine dynamic equation (2) forward in time using a variable-step integrator. Uncertainty in the rotation rate passed to the controller is simulated by a logic block that can add noise to the actual rotation rate (representing an inaccuracy in the controller's inherent estimate for rotation) and attempt to improve the estimate through filtering.
The simulation was adapted to accommodate RivGen®, TidGen®, and the flume turbines. In simulation, inflow time series for each turbine were obtained from ADV measurements, filtered by a cut-off frequency defined by the turbine bandwidth (i.e., the frequencies of motion to which the turbine power generation is sensitive).

- RivGen® turbine: measurements from the turbine deployment site in Iguigig, Alaska

- TidGen® turbine: measurements from Admiralty Inlet, WA as a general proxy for tidal energy deployment sites
- Flume turbine: measurements from the laboratory flume

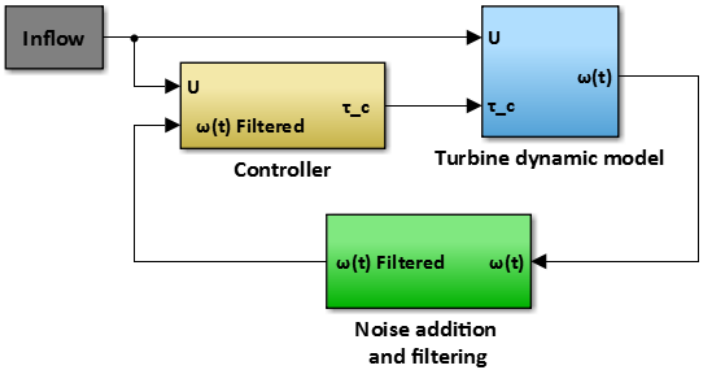

Figure 6: Simplified schematic of Simulink controller architecture.

Turbine parameters used in simulation are presented in Table 11. This section focuses on developing hypotheses for the root cause of the unexpectedly low performance of the TidGen® turbine and implications for controllers for the RivGen® turbine. These methods are revisited in later sections of this report to explain observed behaviors or evaluate hypothetical changes to the turbines (e.g., turbine with elevated moment of inertia).

Table 9: Turbine parameters in simulation

	Flume Turbine	RivGen® Turbine	TidGen® Turbine
Rotor radius [m]	0.086	0.7	1.4
Rotor length [m]	0.234	4.1	10.5
Number of rotors	1	2	2
Swept area [m^2]	0.040	11.5	59.1
Moment of inertia [kg m^2]	0.005	278	2722
Damping coefficient [N m s]	0.003	17	100

As discussed, the TidGen® turbine was unable to operate at peak efficiency despite the implementation of a theoretically effective $K\omega^2$ controller. It was hypothesized that performance was hindered by a noisy measurement of ω. The TidGen® turbine controller was, therefore, implemented and tested with variable update rates and levels of angular velocity signal noise contamination. Further, a filter was implemented on angular velocity estimate used by the controller to evaluate the potential for counteracting noise contamination.

For each additional controller tested (e.g., PI-ω), a parameter sweep was conducted to evaluate the effect of parameters on turbine performance and stability. Controller gain, update rate, filter cut-off frequency, and noise contamination level were explored. Results are tabulated in terms of E_{loss} and the gain or set-point level at which this performance was achieved.

Due to attenuation of high frequencies, each filter requires a certain initialization time at the start of simulation for the mean value of the filter output to approach that of the input. The length of this transient is inversely proportional to filter cut-off frequency. To avoid simulation instabilities as a result

of this transient, the angular velocity signal passed to the controller was switched to the filtered velocity only after the mean value had stabilized. Switching time was maintained at 100 s, corresponding to the stabilization time of the lowest cut-off frequency considered, so that simulations employing different levels of filtering could be fairly compared.

Finally, a criteria for operation at low λ must be set, as there exists a critical value at which there is a high probability the turbine will stall and below which the turbine will immediately stall. For most cases, a conservative stall criteria was selected. Based on previous measurements of the TidGen® turbine and field measurements of the RivGen® turbine in 2015, if the instantaneous tip speed ratio fell below a critical value of 1.5, the turbine was assumed to come to a stop. This is pessimistic, since stall will not occur instantly at this value, but is a reasonable worst-case estimate for performance stability.

The simulation models are provided in the Marine Hydrokinetic Data Repository as a data deliverable from this project.

3.3.2.12 Controller performance from simulation

Initial simulations were conducted for $K\omega^2$, PI-ω, and PI-λ controllers at a 32 Hz update rate, the fastest available high-fidelity ADV time series for each flow condition. These controllers were tested for the RivGen® and TidGen® turbines, as well as the flume turbine (Table 11). For each turbine and controller, a simulation was conducted for which the angular velocity signal was unaltered (referred to as the "Base" case), added Gaussian noise with a variance of 100% the mean angular velocity (abbreviated in table as "N"), and noise addition with filtering ("F+N"). The latter case corresponds to an approach that could improve controller performance in the case of inherently noisy controller input. Five minutes of turbine operation were simulated. Energy loss for each case is summarized in Table 12. For the RivGen® and TidGen® turbines, the addition of noise to the controller input significantly degrades turbine performance. Variations in base case energy loss between the turbines are caused by differences in relative losses from drivetrain damping in each system. The flume turbine, with higher relative damping, has a relatively high base case energy loss despite operating stably at a nearly ideal set point. The higher relative damping of the flume turbine is also the reason that it is less sensitive to noise.

Table 10: Simulated energy loss for RivGen®, TidGen®, and flume turbines under PI-ω, PI-λ, and $K\omega^2$ controllers with added noise (N) and filters (F+N).

	PI-ω			$K\omega^2$			PI-λ		
Turbine	**Base**	**N**	**F+N**	**Base**	**N**	**F+N**	**Base**	**N**	**F+N**
RivGen	3.9	20.3	20.3	2.6	16.0	5.9	3.6	14.5	14.6
TidGen	4.1	28.3	28.3	0.8	34.1	4.8	1.6	32.0	32.1
Flume	25.4	25.9	25.5	25.3	25.9	25.5	25.4	26.0	26.0

The variations in other controller parameters of interest: angular velocity, tip speed ratio, and command torque are shown in Figure 7- Figure 9.

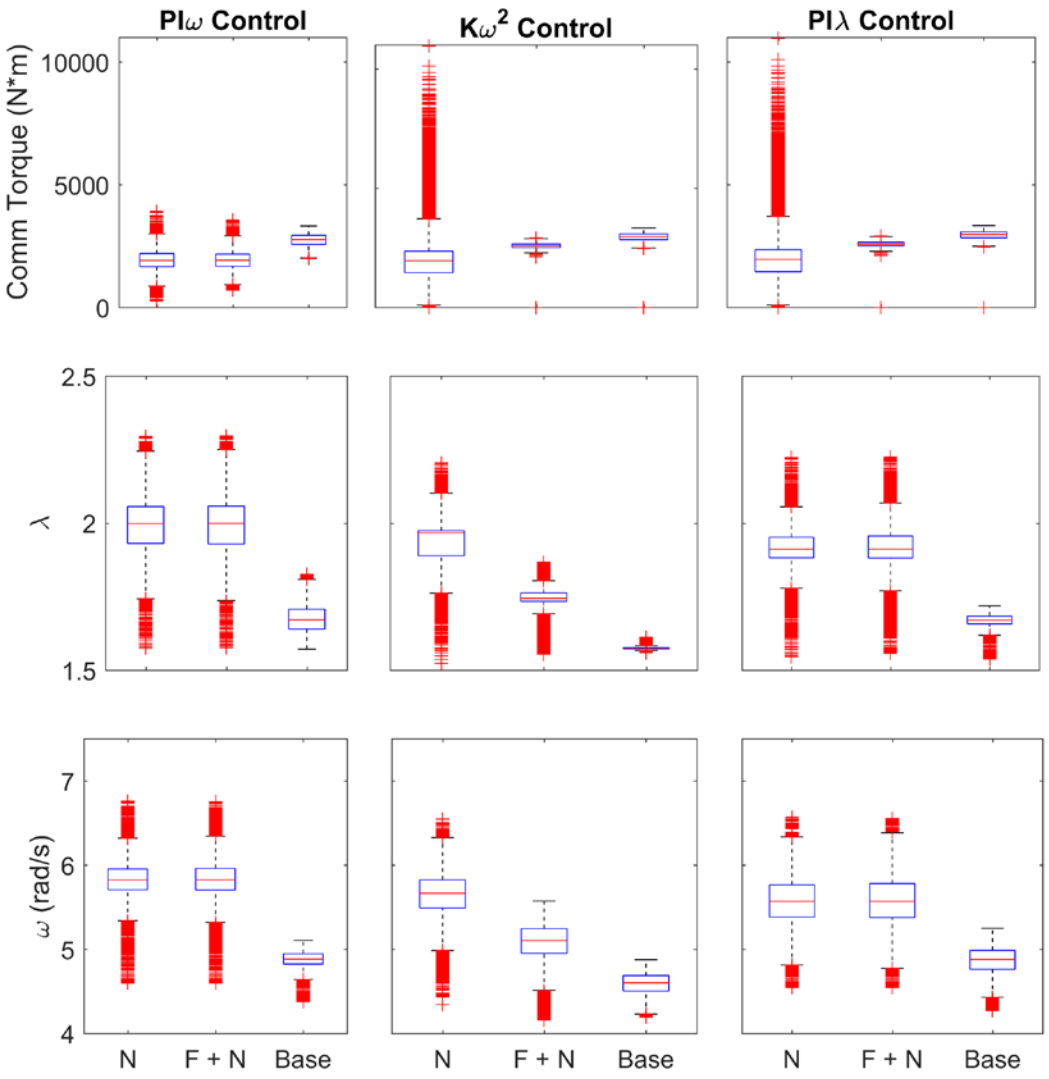

Figure 7: Box plot of RivGen® simulation results demonstrating the effects of noise addition and filtering. The base case is represented by "Base". Response of system with noise added to the omega signal is given under case "N". Added noise and applied filter response is given by "F + N".

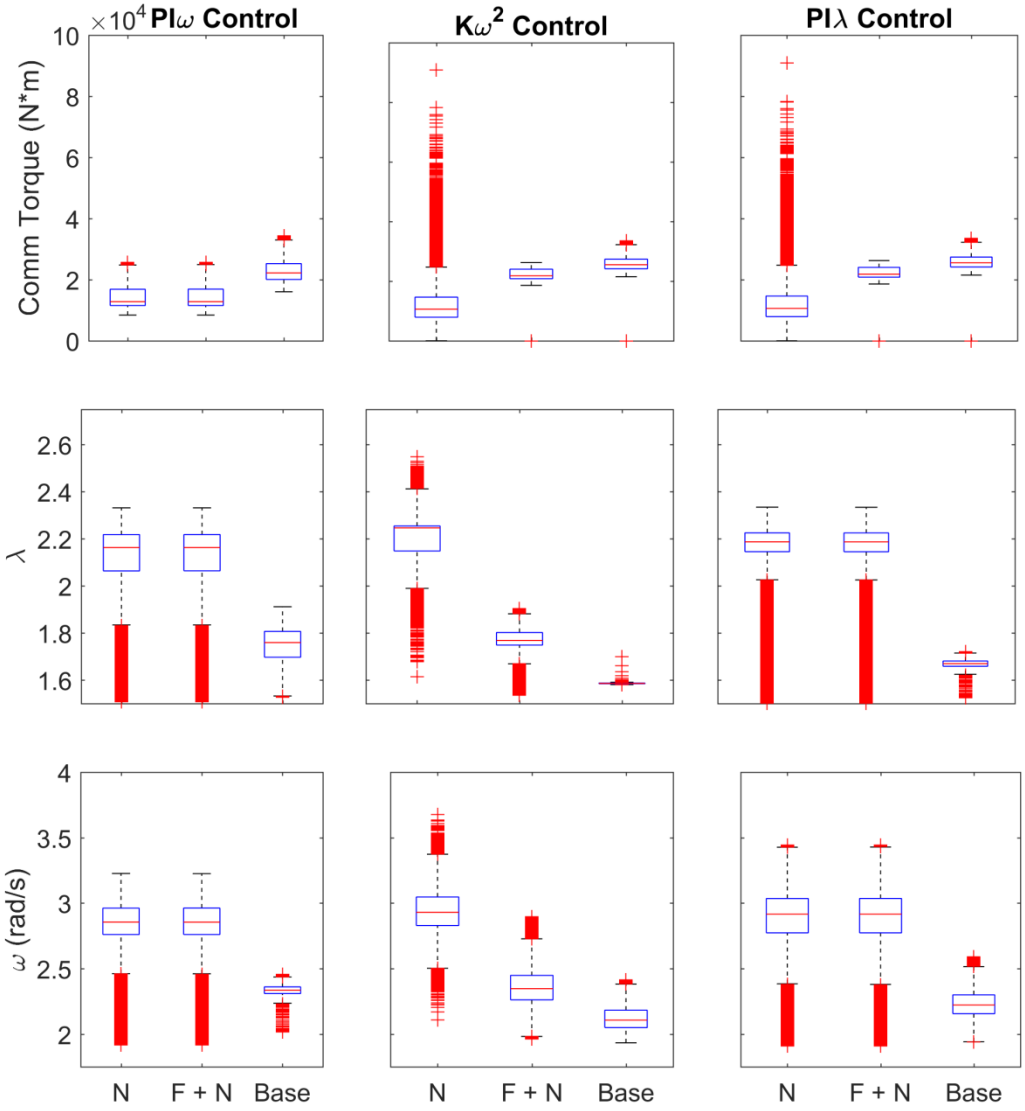

Figure 8: Box plot of TidGen® simulation results demonstrating the effects of noise addition and filtering. The base case is represented by "Base". Response of system with noise added to the omega signal is given under case "N". Added noise and applied filter response is given by "F + N".

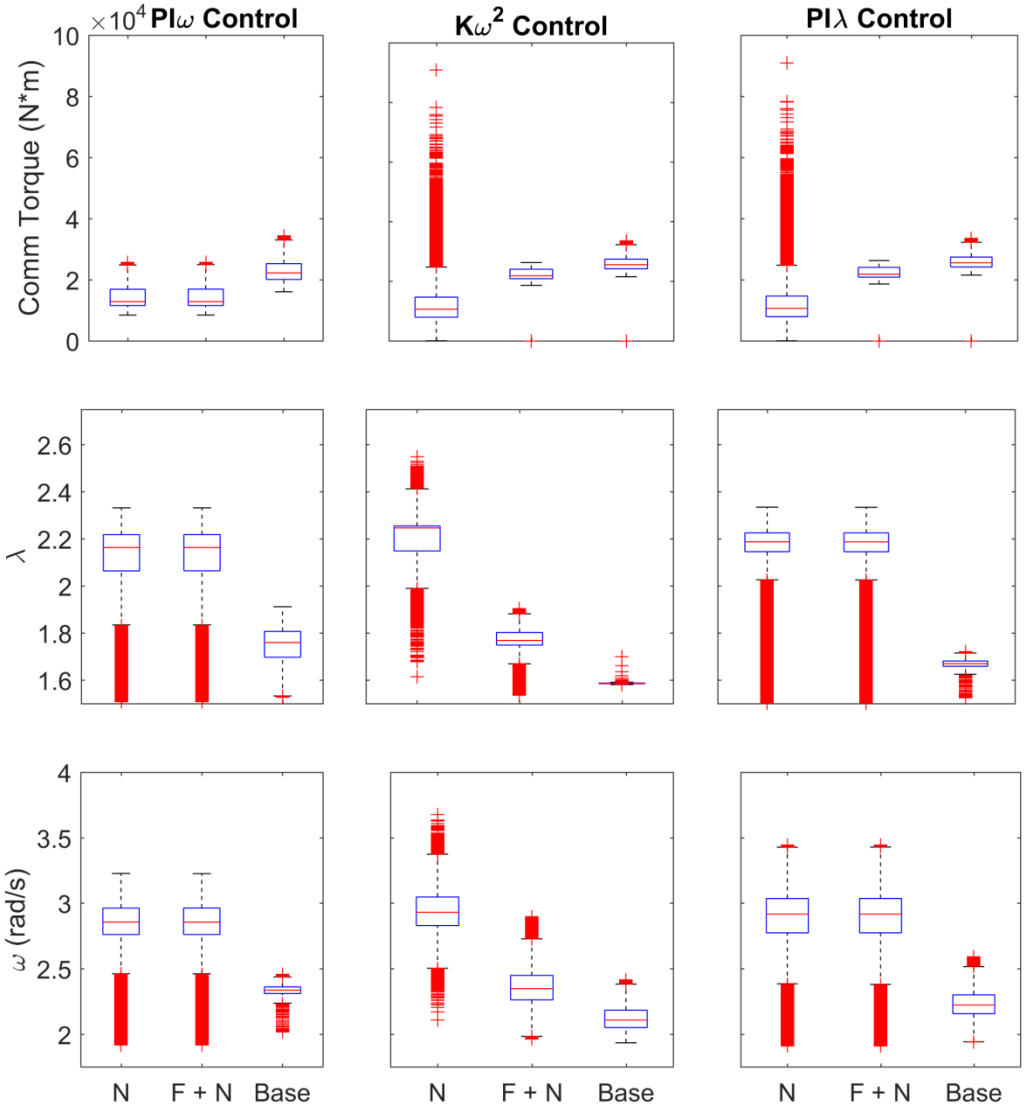

Figure 9: Box plot of the flume turbine simulation results demonstrating the effects of noise addition and filtering. The base case is represented by "Base". Response of system with noise added to the omega signal is given under case "N". Added noise and applied filter response is given by "F + N".

For the RivGen® and TidGen® turbines, simulations suggest that the $K\omega^2$ controller has the lowest E_{loss}. Further, the performance of all controllers, in terms of energy loss, torque demands, and set point holding, are diminished with the addition of significant noise. With the strict stall criteria used in simulation, the addition of a filter to the linear controllers is not effective at recovering base case performance. However, the performance of the $K\omega^2$ controller is substantially improved with the addition of a filter on a noisy input signal.

All controls architectures were more sensitive to the introduction of a phase shift by the filter than residual noise, and the linear controllers were found to be much more sensitive to this than the $K\omega^2$ controller. As a result, the best-performing filter for the linear controllers was a 1st-order Butterworth

filter with a cut-off frequency that was a significant fraction (i.e., 1/2, 1/4) of the Nyquist frequency. Lower cut-off frequencies tended to increase the required set point for stable operation, increasing energy loss, but smoothing the control torque demands. For noise-added cases, linear controllers required gain values 1 to 2 orders of magnitude below ideal gains to maintain stability, further reducing their ability to maintain set points. The $K\omega^2$ controller showed the highest performance when a 1st-order Butterworth filter was applied with a cut-off frequency well below the turbulent kinetic energy peaks for the inflow time series (0. 1 Hz for RivGen® and TidGen®, 1 Hz for the flume turbine).

3.3.2.13 Controller update rate

Controller performance was found to be highly sensitive to update rate, even in the absence of noise contamination. The effect is more pronounced for the feedback controller (PI-λ) than feedforward controller ($K\omega^2$). As shown in Figure 10, update rates faster than 10 Hz show diminishing returns for the RivGen® turbine.

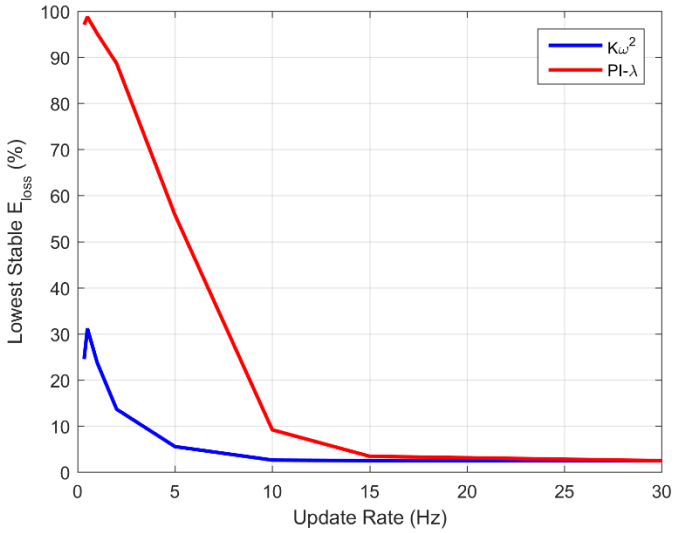

Figure 10: Effect of controller update rate on RivGen® turbine energy loss for two controllers. Feedback controls requires a faster update rate to ensure low Energy Loss.

The turbulent kinetic energy spectra and generator power spectra (following frequency analysis from Thomson et al. 2012) measured during the RivGen® deployment in Iguigig, Alaska (Figure 1) shows that there is limited energy in the turbine power output at frequencies faster than 0.2 Hz, which is unsurprising, given that there is limited energy in the turbulent inflow above 0.15 Hz.

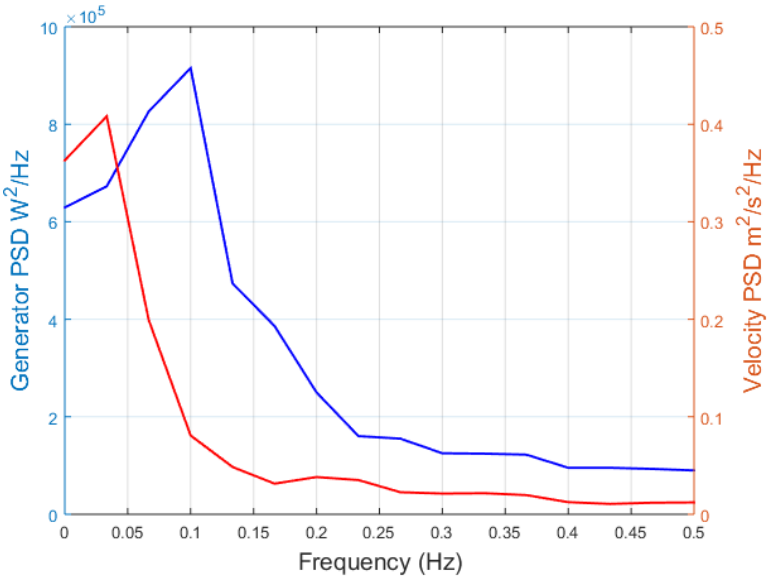

Figure 11: The free-stream velocity and generator power spectra for the RivGen® turbine in Igiugig (2014 measurements). The velocity data are acquired at 16 Hz, while the generator power data is logged at 1 Hz, resulting in a broader bandwidth for the electrical power spectra. The generator is capable of responding to the change in energy in the flow.

3.3.2.14 Filtering and noise addition

The effects of noise-contaminated angular velocity signals were investigated as an explanation for the performance limitations observed for TidGen® turbine operations in Eastport, Maine. The TidGen® $K\omega^2$ controller updated at a rate of 2000 Hz, substantially faster than the highest energy-containing frequencies of turbulence in tidal channels (Thomson et al. 2012). Initial tests added a normally-distributed random variable with a given variance to the angular velocity signal. At optimal rotation rate in a current of 1.4 m/s, the TidGen® turbine rotates at 1.7 rad/s.

Table 11: Effect of controller noise on TidGen® turbine performance. E_{loss} and gain ratio (Section 3.3.2.9) are shown for maximum stable (non-stalling) turbine performance. The unfiltered case with the highest noise level stalls immediately at all tested gains.

Rotation Rate Noise Variance (σ^2) ($rads^2/s^2$)	No Filtering		1st Order Butterworth Filter (cut-off 0.01 Hz)	
	E_{loss} (%)	Gain ratio (K/K*)	E_{loss} (%)	Gain ratio (K/K*)
0	1	1	2	0.83
0.05	2	0.83	2	0.83
0.1	4	0.70	2	0.83
0.25	9	0.57	2	0.83
0.5	15	0.43	3	0.78
1.0	20	0.35	4	0.74
2.0	34	0.22	5	0.70
4.0	-	-	6	0.65

As shown in Table 13, if there is no noise in the estimate for ω, the controller almost perfectly tracks the energy-containing turbulent motions in the flow and residual E_{loss} is caused by power train damping (B). However, sensor noise can significantly degrade turbine performance. This suggests that the TidGen® turbine performance shortfall could be explained by a noisy control signal. Since this hypothesis could

not be verified without dynamometer testing of the TidGen® generator, a variety of filters were tested in simulation to explore measures that could mitigate the effect of sensor noise. A parameter sweep of filter morphologies indicated that the turbine, though susceptible to the degree of noise, could be more seriously impacted by phase-shifts in the control signal introduced by filters, as shown in Table 14 for the higher order filters with higher frequency cut-offs.

Table 12: Simulated E_{loss} [%] for TidGen® turbine in peak tidal flow (1.9 m/s mean velocity) under Kω^2 control with various filters and added noise.

Rotation Rate Noise Variance (σ^2) [rads^2/s^2]	No Filtering	10th Order Butterworth, 2 Hz cut-off	4th Order Butterworth, 0.5 Hz cut-off	1st Order Butterworth, 0.5 Hz cut-off	1st Order Butterworth, 0.01 Hz cut-off
0.25	9	14	11	4	2
0.5	15	20	14	6	3
1.0	20	27	20	9	4
4.0	-	45	33	23	6

A first order Butterworth filter with a cut-off frequency of 0.01 Hz is effective at attenuating high-frequency noise without significantly phase-shifting controls inputs within energy-containing frequencies (< ≈0.2 Hz), as shown in the right hand columns of Table 13. Note that for low-noise or noiseless estimates of ω, the filtered control signal results in worse performance than the unfiltered case. This suggests that for a system in which there is little to no noise contamination in the angular velocity signal, filtering may actually degrade performance. In any case, overly aggressive filtering renders the turbine unresponsive to energy-containing disturbances in the mean flow.

3.3.2.15 Laboratory testing of turbine system

Laboratory experiments were carried out at the Marine Sciences Centre in Bamfield, BC, Canada. The recirculating current flume at this facility can produce flow velocities in excess of 1.0 m/s, and is equipped with a chiller to maintain water temperature during operation. This ensures that the water had consistent properties during long test periods, and avoids complications that can arise from Reynolds number variations associated with temperature changes.

The primary objective of the experiments is to explore simulated control architectures on an actual turbine, and use the results to design controllers for a full-scale turbine. For results to scale accurately between turbines, their dynamic response to controls inputs and turbulent perturbations must be similar. For turbines with identical performance curves, similarity can be achieved by matching the ratio of turbine moment of inertia to damping, *J/B* (i.e., the turbine time constant) (Cavagnaro et al. 2015).

Because torque varies non-linearly with operating point λ, as defined by the performance curve, it is not possible to ensure dynamic similarity by merely matching the *J*/*B* ratio for turbines with dissimilar performance curves. This is the case for the RivGen® turbine and the flume turbine, which have relatively different performance curves. However, the effect of noise on a given control architecture can be scaled by considering the relative magnitude of change in angular velocity brought about as a result of an erroneous control signal.

For the RivGen® turbine and the flume turbine in identical inflows shows that the laboratory-scale turbine is more resilient to noise across the operable range of tip speed ratios, which is consistent with the results from simulation results in Table 12. Because the laboratory-scale turbine is much less

sensitive to noise than the RivGen® turbine, noise levels in the flume were intentionally elevated to the levels needed to cause a turbine response commensurate with that of the RivGen® turbine. Noise levels with a variance ranging from 50 to 250 rad^2/s^2 were found in simulation to create disparities in energy loss that would likely be measureable experimentally. Thus, the relative effectiveness of a given controller/filter strategy could be fairly evaluated in the context of its effectiveness on the full-size device.

The experimental turbine is a four-bladed helical turbine with 90^o swept blades based on a NACA0018 airfoil with a 6^o preset pitch angle (positive, leading edge titled out) defined at the quarter-chord length. Preliminary tests were used to estimate a turbine damping coefficient from torque measurement under no load conditions (free-wheel). Precise determination of the turbine's rotational moment of inertia is confounded by added mass when accelerated. However, the moment of inertia estimated from acceleration tests in quiescent water compared favorably to an analytical static estimate based on the turbine's geometry and mass. A damping coefficient was estimated by allowing the turbine to freewheel ($\tau_c = 0$). In this state, frictional losses in the system due to damping equal hydrodynamic torque production, and can thus be determined via direct measurement. This suggests that added mass is a second order effect for the laboratory turbine. Flume turbine properties are summarized in Table 15 with equivalent properties for the RivGen® turbine provided for context.

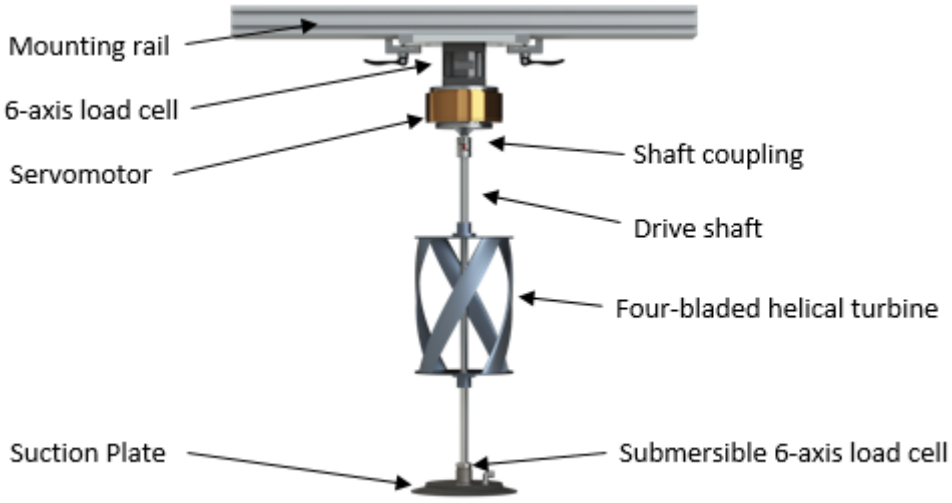

Figure 12: Rendering of University of Washington turbine and laboratory instrumentation

Table 13: Flume and RivGen® turbine properties

Property	Flume Turbine	RivGen Turbine
Moment of Inertia (*J*)	0.005 kg m^2	278 kg m^2
Rotor Radius (*R*)	0.086 m	0.7 m
Rotor Length (*L*)	0.234 m	4.1 m
Number of Rotors	1	2
Area (*A*)	0.040 m^2	11.5 m^2
System damping[2] (*B*)	0.003 N m s	17 N m s
Time Constant (*J/B*)	2 s	16 s

The Bamfield Marine Sciences Centre flume has a cross-sectional area of 0.98 m x 0.75 m with a working length of 10 m. The test assembly was roughly centered in this working length. For this flume and test rig, the blockage ratio is 6.7% and is low enough to not significantly affect turbine performance. Controller tests were conducted at 1 m/s. At this speed, results were statistically stationary after 30 seconds of observations.

After taking tare measurements for both load cells and aligning the drive shaft in a static flume, pumps were enabled and the flume was allowed to come to reach a steady state speed of 1 m/s speed. The turbine was then allowed to accelerate to freewheel. After the turbine reached a steady rotation rate, the controller was activated and used to step the turbine through various gain levels, filter configurations, noise levels, and/or set points. Each set point was held for 30 s, after which the resistive torque was released, the turbine was allowed to return to freewheel, and the next gain setting was applied. When all settings had been tested, the pumps were shut down and the flume was allowed to settle before a second tare level was obtained for all sensors, to correct for instrument drift during the tests.

3.3.2.16 Laboratory performance of non-adaptive controllers

Initial tests were performed to develop the curve for the turbine by automatically stepping through torque set-points under constant inflow. This brought the turbine through a range of tip-speed ratios from freewheel (no resistive torque applied) to stall. The performance curves for the flume turbine for a range of inflow speeds are shown in Figure 13. Note that the performance curve is not independent of inflow speed, indicating that turbine performance is not independent of the Reynolds number. However, this has little effect in the low-turbulence flume environment when operated a constant mean velocity.

[2] The tabulated damping refers to the damping of the entire test assembly, including damping associated with the servomotor.

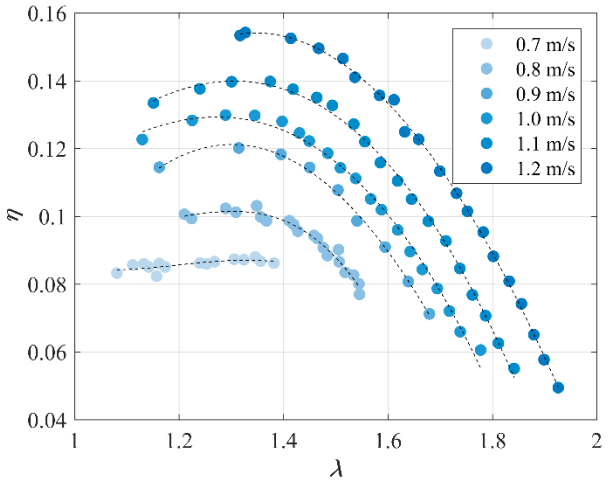

Figure 13: Laboratory-scale turbine performance under torque control at different inflow speeds.

A summary of performance curves for each non-adaptive controller operating with and without added noise is shown along with the performance curve at 1 m/s inflow velocity in Figure 14. Gain or set point runs that resulted in turbine stall are not included.

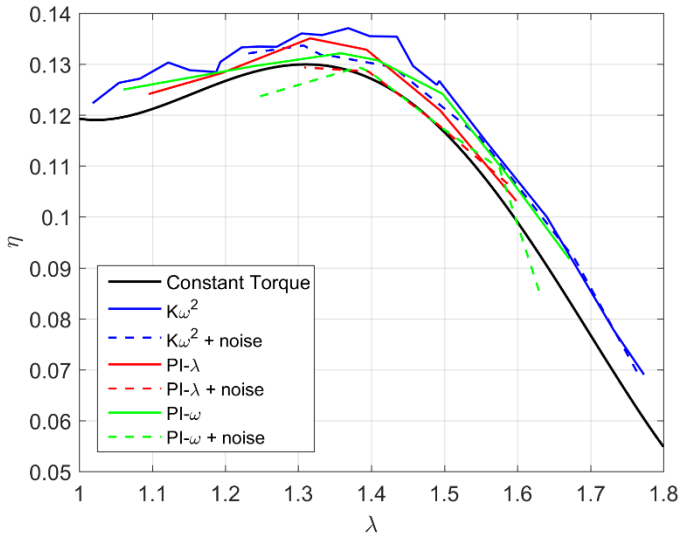

Figure 14: Efficiency vs. tip-speed ratio for each controller with and without noise addition.

Although there was some variability between runs, even noise contaminated controllers were able to operate the flume turbine stably at the peak of the performance curve. Because of this, energy loss values for ideal set points, calculated by integrating efficiency over the duration of the test run, do not change significantly with noise addition (Table 16). This is because the performance curve is relatively flat near its peak, and the peak is relatively far from the turbine stall point ($\lambda < 1.1$). Consequently, erroneous control actuation due to a noisy angular velocity measurement was insufficient to bring about turbine stall or significantly reduce energy capture. In general, an actively controlled turbine tended to slightly outperform the constant-torque performance curve.

Table 14: E_{loss} [%] for laboratory experiments[3]

Controller	Baseline	Added Noise	Added Noise and Filtering
PI-ω	5	7	-2
$K\omega^2$	2	3	0
PI-λ	4	3	3

For the noise-contaminated $K\omega^2$ controller, the squaring of the added Gaussian noise to the angular velocity signal causes a mean-shifted control torque. Consequently, the peak of the performance curve was obtained for noise-contaminated cases at lower *K* values than suggested by theory.

Adding noise to the angular velocity signal reduces the stability of all controllers as the tip-speed ratio approaches the point of stall and filtering the controller input signal mitigates this effect. As for $K\omega^2$ simulation, the most effective filters were found to be first-order filters with low cut-off frequencies on the order of the most energetic turbulent frequencies in the flume (1 Hz). This relatively low cut-off frequency performed well for linear controllers, as well.

The ability to hold a set-point and command torque ranges are also adversely affected by noise addition. As shown in Figure 15, filtering the noise-contaminated signal is similarly effective in correcting this.

[3] Due to the non-linear relationship between commanded torque and servo-applied torque, experimentally determined energy loss values are calculated using the measured torque, which captures system damping that would be other considered a loss. Consequently, energy loss values are much lower than in simulation of the laboratory turbine.

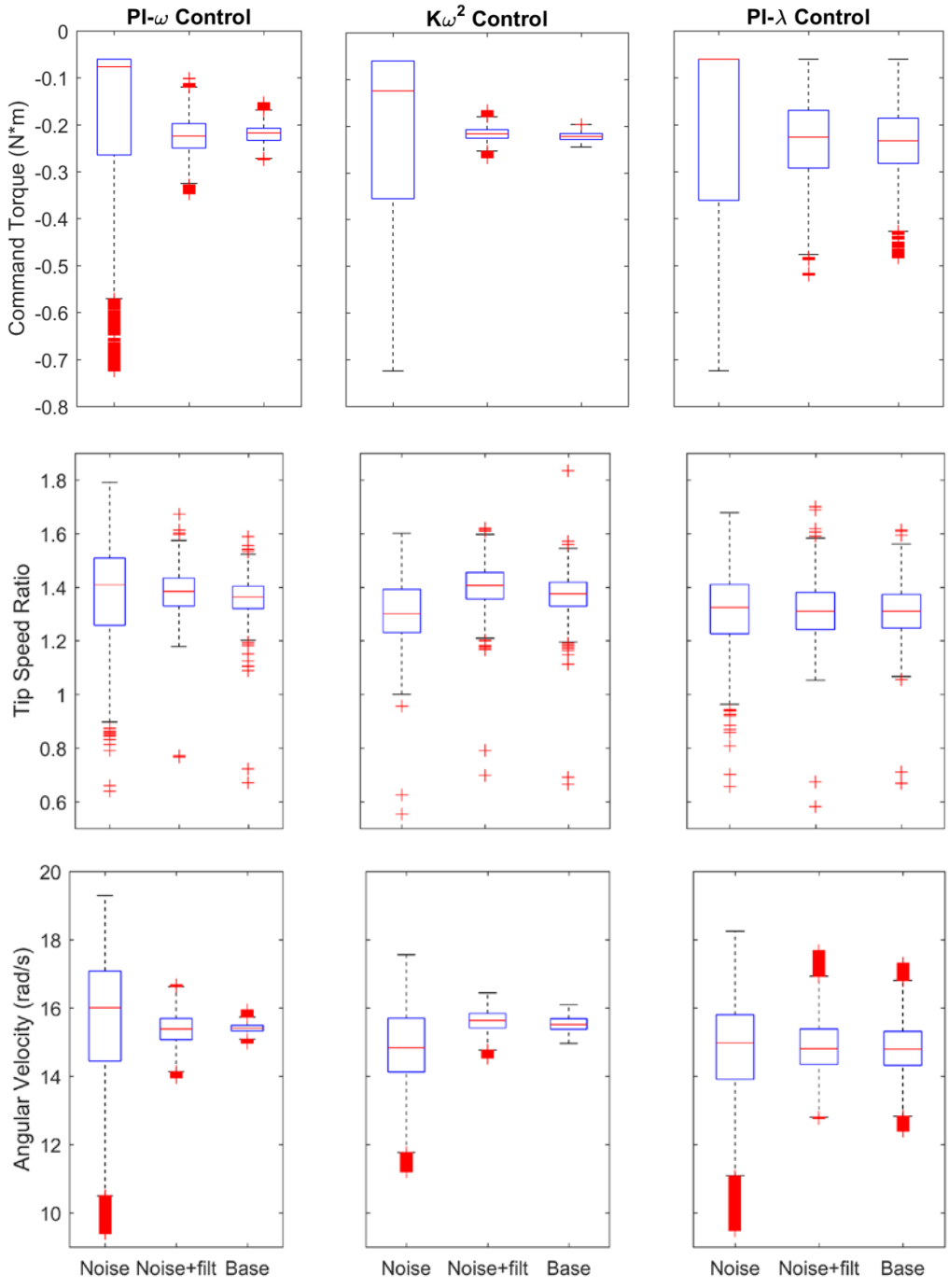

Figure 15: Box plots for added noise, noise and filtering, and base (no added noise or filters). The median, 1st and 3rd quartiles, and minimum/maximum values that are not outliers are shown as horizontal red lines. Outliers are shown as red +. The base case is represented by "Base". Response of system with noise added to the omega signal is given under case "N". Added noise and applied filter response is given by "F + N".

The $K\omega^2$ controller, when filtered, commands a significantly smaller range of generator torques than PI-ω or PI-λ controllers and results in superior set point holding. Somewhat counter intuitively, the PI-λ controller is not able to hold tip speed ratio set point as effectively as the PI-ω controller. However, for the low-turbulence inflow, it is likely that the added complexity of the upstream speed measurement

using the ADV and the assumption of coherent turbulent structures advecting with the flow (i.e., Taylor's hypothesis) introduces more uncertainty and error into the control algorithm than benefit gained by tracking the minimal turbulence. The PI-λ controller was less affected by noise in terms of holding both angular velocity and tip-speed ratio set points than the PI-ω controller. Because PI-λ control depends evenly on two sensor inputs to determine control actuation, and only the angular velocity signal is contaminated with excess noise, the effect of this noise will be reduced except when it is in-phase with a random fluctuation in ADV signal, decreasing overall noise sensitivity.

3.3.2.17 Laboratory performance of adaptive nonlinear controller

Flume tests of the adaptive nonlinear controller were similarly conducted. However, the turbine was subjected to variable inflow speeds between 0.7 m/s and 1.2 m/s by varying pump settings at predetermined times throughout 300 s trials. Control torque was adjusted to maintain the maximum power-point according to the performance curves shown in Figure 13 by evaluating a quadratic polynomial fit to controller gain K with ADV measurements of U. E_{loss} was used as a metric to evaluate the controller's effectiveness and compared to control with constant K gains corresponding to points lower than, higher than, and at the maximum power-point for the mean inflow speed over the 300 s test.

The adaptive nonlinear controller (adaptive $K\omega^2$) successfully maintained stable operation through changing inflow speed. Results of the testing are compiled in Table 17. Each of the controllers produced a negative E_{loss}, indicating they performed better than the expected maximum efficiency based on the pre-defined performance curves. This is hypothesized to result from the performance increase from high-frequency torque oscillations (an unintended consequence of closed loop torque control), as well as uncertainty in performance curves. Additionally, the adaptive controller did not outperform a constant gain controller with a gain optimized for the mean of the 300 s inflow time series. However, in a field implementation of this controller, if system performance is a strong function of velocity and/or a large range of velocities are encountered (as in a tidal system), the adaptive method is expected to yield better results. A typical time-series of instantaneous turbine efficiency compared to expected maximum efficiency is shown in Figure 17, along with the velocity time series for the adaptive control cases.

Table 15: Performance of adaptive nonlinear controller

Gain Optimization	K	E_{loss} [%]
Adaptive	Adaptive (4E-4 – 8E-4)	-26
Velocity lower than actual mean	4E-4	-1
Actual mean	7E-4	-26
Velocity higher than actual mean	8E-4	-23

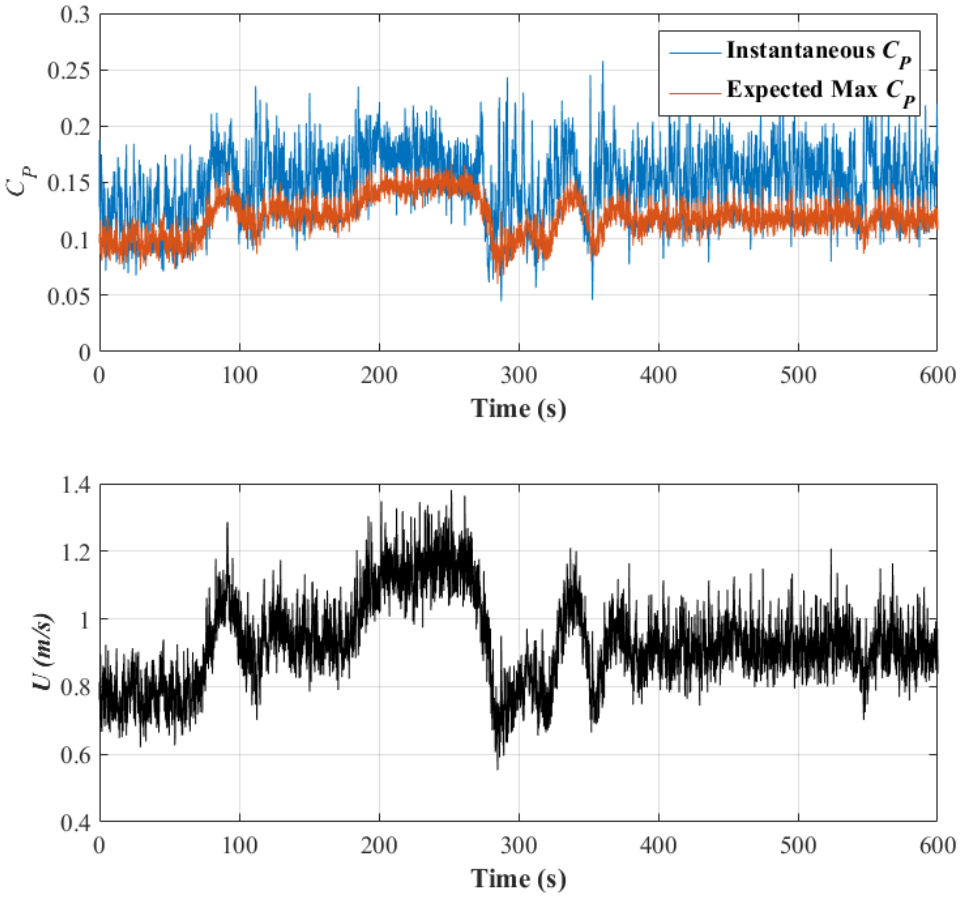

Figure 16: Typical adaptive nonlinear controller performance. For a given inflow, U, variation in Cp results.

3.3.2.18 Effect of elevated turbulence in laboratory testing

To test the performance of the PI-ω and $K\omega^2$ controller in the presence of a more realistic turbulence, a cylinder was suspended vertically 6 diameters upstream of the turbine so that it occupied the entire depth of the flume. The diameter of this cylinder was selected according to U. Fey, M. König, & H. Eckelmann (1998) to produce vortices that would engulf the turbine. The 6 cm diameter cylinder shed vortices at 3 Hz, which, advecting in a 1 m/s flume, corresponds to a length scale of 0.33 m, engulfing the 0.17 m diameter turbine. Because the velocity measured by the ADV would be affected by formation and propagation of these vortices, it could not be used for to provide an accurate estimate of inflow velocity. Consequently, the PI-λ controller could not be tested with elevated turbulence.

The controllers performed well in synthetic turbulence produced by a cylinder positioned upstream of the turbine. As expected, the PI-ω controller had to exercise a broader range of control torque than the $K\omega^2$ controller to maintain a fixed angular velocity in the more turbulent environment. The $K\omega^2$ controller showed a larger range of angular velocities during operation because it was attempting to maintain a performance set point in the turbulent inflow. The presence of a filter (1^{st} order Butterworth with cut-off frequency of 1 Hz) on the estimate for ω did not significantly affect the operation of either tested controller (Figure 18), which would be expected given that the filter is constructed to pass most of the energy-containing velocity time scales.

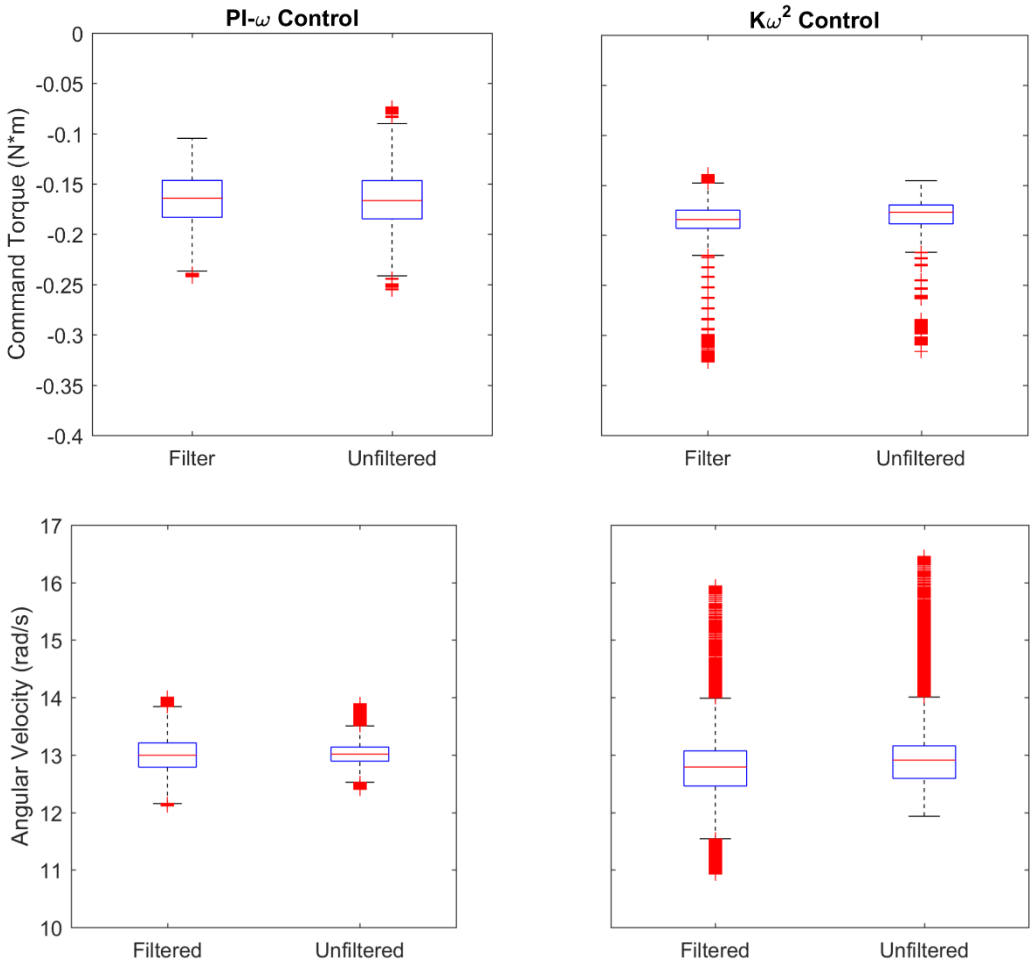

Figure 17: Box plots for PI-ω control (left) and Kω^2 control for added turbulence tests.

3.3.2.19 Emulation of turbine power takeoff

Evaluating the power takeoff (PTO) components and control architecture of a field-scale hydrokinetic turbine involves many challenges. Foremost among these is the cost associated with commissioning and deploying systems in the field. Fortunately, electromechanical emulation machines (EEMs) have been shown capable of mimicking the dynamic performance of a hydrokinetic turbine in a laboratory environment and allow the development of a PTO and control strategy prior to field deployment (Cavagnaro et al., 2015). An EEM typically consists of an instrumented and controllable motor-generator set. The motor, or 'prime mover' of the system is programmed to behave as a turbine, and is capable of dynamically reacting to a prescribed inflow speed time series and resistive torque applied by the generator. The generator provides a load in response to control commands based on a desired governing scheme. Generated power can be dissipated or returned to the grid, depending on available configurations.

An EEM at the MaREI-Beaufort test center in Cork, Ireland was utilized to emulate the RivGen® turbine and evaluate several aspects of PTO integration and control. A full description of the work was presented and published in the Proceedings of the 11th European Wave and Tidal Energy Conference, Nantes, France, Sept. 2015.

The 'Conn' EEM at MaREI-Beaufort is rated for 22 kW and consists of a squirrel cage induction motor controlled by a programmable motor drive as its prime mover and a wound rotor induction generator electrically coupled to a controllable back-to-back motor drive configuration. The generator drive arrangement allows power to be returned to the grid in a regenerative mode; a generator-side power converter provides a variable-speed load, resulting in variable frequency power which is converted to DC and exported to the grid-side drive, boosting and inverting the DC to grid frequency and voltage. Sensors on the EEM provide feedback for rotation rate (ω_m), generator torque (τ_g), and instantaneous RMS power (P_g).

3.3.2.20 Turbine emulation

The prime mover controller utilized two primary user inputs to direct the induction motor to act as a turbine: the turbine's performance curve and inflow speed. Given turbine parameters of rotational moment of inertia (J), damping coefficient (B), area (A), and radius (R), the performance curve ($C_P(\lambda)$) was polled at each time-step of emulation to determine hydrodynamic torque (τ_h) as a result of the inflow speed (U) and turbine rotation rate (ω). U was a simulated turbulent time series produced by TurbSim at a representative inflow mean of 2.0 m/s. After initialization, subsequent values of ω were solved for by numerically integrating the dynamic equation of motion for turbine rotation,

$$\dot{\omega} = \frac{1}{J}(\tau_h - B\omega - \tau_c)$$

in which τ_c is resistive torque as the result of PTO loading. A motor speed command is determined from emulated turbine speed as,

$$\omega_m = N_v \omega$$

where N_v is a virtual gearbox ratio used to align the low speed, high torque characteristics of the turbine with the high speed, low torque characteristics of the prime mover. The speed command was enacted by the motor drive with an internal closed-loop speed controller.

3.3.2.21 Generator control emulation

The generator side drive provided a resistive load (τ_g) to the generator such that

$$\tau_g = \frac{\tau_c}{N_v}$$

Commanded torque, the control variable for the system, was derived from the control strategies evaluated. These included: $K\omega^2$, PI-λ, PI-ω, and a constant resistive control similar to loading utilized during 2014 field tests of the RivGen® turbine to allow for direct comparison and validation of the methods. All torques in the system (determined hydrodynamic and commanded load) as well as J and B were scaled by 50% to allow for high torque/current transients resulting from turbulent gusts to be resolved. Therefore, output power from the EEM was modeled at 50% of full scale, while rotational dynamics between emulation and field testing were maintained.

3.3.2.22 Effect of update rate on controller stability in emulation

The update rate of control torque applied by the generator was investigated to determine a lower limit for stable operation. The prime mover updated emulated turbine rotation according to (5) and recorded feedback from sensors at a rate of 100 Hz. Inflow speed was prescribed at 16 Hz and a zero order hold was utilized to maintain speeds during intervening time steps. A 1 Hz update rate for control action resulted in unstable performance, as large control actions (limited by the EEMs current capability) were applied at each update in an attempt to achieve the desired set-point. Oscillation between extremes of

commands resulted in tripping the generator drive. A 10 Hz update rate for control action was found to be stable for all controllers evaluated.

3.3.2.23 Controller performance in emulation

The remaining controllers evaluated attempted to maintain operation at the turbine's maximum power point ($K\omega^2$, PI-λ) or hold a constant rotation rate optimized for the average flow speed of the 300 s input time series (PI-ω). The maximum power point tracking controllers performed similarly in terms of emulated turbine efficiency, with the $K\omega^2$ controller providing lower variance of control torque. The PI-ω controller was unable to maintain optimal power in response to turbulent changes in inflow speed, as expected. However, when total system efficiency including that of the generator (η_s) was evaluated, all three controllers were grossly equivalent (Figure 20). This is because the EEM's generator is slightly more efficient under constant speed operation, compensating for the reduction in mechanical power produced by the rotor at non-optimal tip speed ratio. This result can be seen in E_{loss} for the controllers per the definition in (8) compared to a variation in which electrical power output appears in the numerator (Table 19).

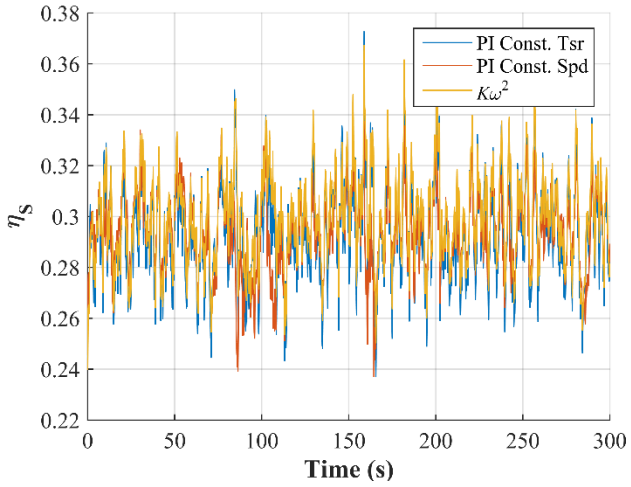

Figure 18: Comparison of emulated system efficiency under various controllers for a 300 s turbulent inflow time series.

Table 16: Performance of controllers in emulation

Controller	E_{loss} [%] - mechanical	E_{loss} [%] - electrical
PI-ω	2.2	5.3
$K\omega^2$	0.5	4.4
PI-λ	1.5	6.7

3.3.3 Problems Encountered and Departure from Planned Methodology

The original hypothesis was that preview information on the flow would provide information, which could be used to precondition the state of the turbine to optimize energy production. Data from field measurements, as outlined below, indicates that the turbulence is relatively slowly evolving and that the hydrokinetic power system is capable of responding quickly enough to fully capture the energy in the flow.

Various control scheme models of the system have been created and validated by both model testing and emulation. These controls schemes include feedback and feedforward controllers.

3.3.4 Assessment of Their Impact on the Project Results

The original hypothesis about the utility of preview control to enhance energy capture in hydrokinetic applications has been shown to be invalid. However, improving the utility of improved control schemes shows promise for increasing energy and power generation. The project objectives of increased energy generation and resulting decrease in cost of electricity are achievable. These findings were presented as part of the Go/No Go decisions process.

3.4 Field Campaign for Turbulence Measurements and Turbine Response

3.4.1 Original Hypotheses

A field campaign was planned to collect turbulent inflow data at the RivGen® TGU site to understand the space and time scales in which inflow information could be projected forward to a turbine. The goal was to develop, on time scales of seconds to minutes, a measurement-based preview of what the inflow will be at the turbine. The deterministic turbulence measurements were to be correlated with co-temporal measurements of power output.

Field measurement was to involve the deployment of existing instrumentation in an array to map streamwise and cross-stream velocity variations with maximum spatial lag combinations. During the field measurements, co-temporal measurements of TGU parameters were to be collected by ORPC. Both the acoustic Doppler current profilers and acoustic Doppler velocimeters used to characterize inflow for feedforward control of the MHK turbine are active acoustic instruments. The operating frequency for the profilers and velocimeters are 1 MHz and 6 MHz, respectively.

The objective of this task was to evaluate and refine uncertainty metrics in flow preview information associated with the time-evolution of the velocity field and uncertainty inherent to the measurement techniques, including an assessment of the adequacy of single beam ADCP measurements to capture the relevant data, and to confirm that the selected component performance metrics can be correlated with flow measurements.

3.4.2 Approaches Used

Two separate deployments of the RivGen® Power System were conducted in the Kvichak River in Igiugig, Alaska. In 2014 the system was deployed and velocity measurements were made by researchers from the University of Washington to assess the variability of the river flow. In 2015 the system was again deployed and control schemes implemented and tested. As part of the 2015 work, the river resource was again mapped and measured.

Velocity measurements during the Ocean Renewable Power Company's RivGen® turbine deployment at Igiugig, Alaska, in 2014 were used to assess the variability of the river flow. The first objective was to understand the spatial variability of the inflow velocities for RivGen®, in particular the strong spanwise shear that occurs at the RivGen® location. The second objective was to understand the time variability of inflow velocities, in particular the streamwise coherence of the inflow velocities. Results suggest that the river flow is approximately steady, in the mean sense, at any particular location in the river, with random turbulent fluctuations that are around 10% of the mean flow. The mean flow in the center channel of the river is 2.5 m/s, with reductions near the riverbanks and in the shallows. As the flow is quasi-steady, the data from various stations can be gridded to a synoptic flow map around the turbine. A cross-section of this flow map immediately upstream of the turbine shows strong inflow velocity gradients across the turbine. Spectral analysis and lagged correlation results indicate that temporal fluctuations at a given point are dominated by large scale fluctuations (> 10 s), such that measurements at the turbine location are just as useful for inflow control implementation as upstream measurements.

The ORPC deployment site on the Kvichak River is just downstream of the village of Igiugig, Alaska. The river is approximately 5 m deep and 150 m wide at the deployment site, and the turbine hub-height is approximately 2 m below the surface.

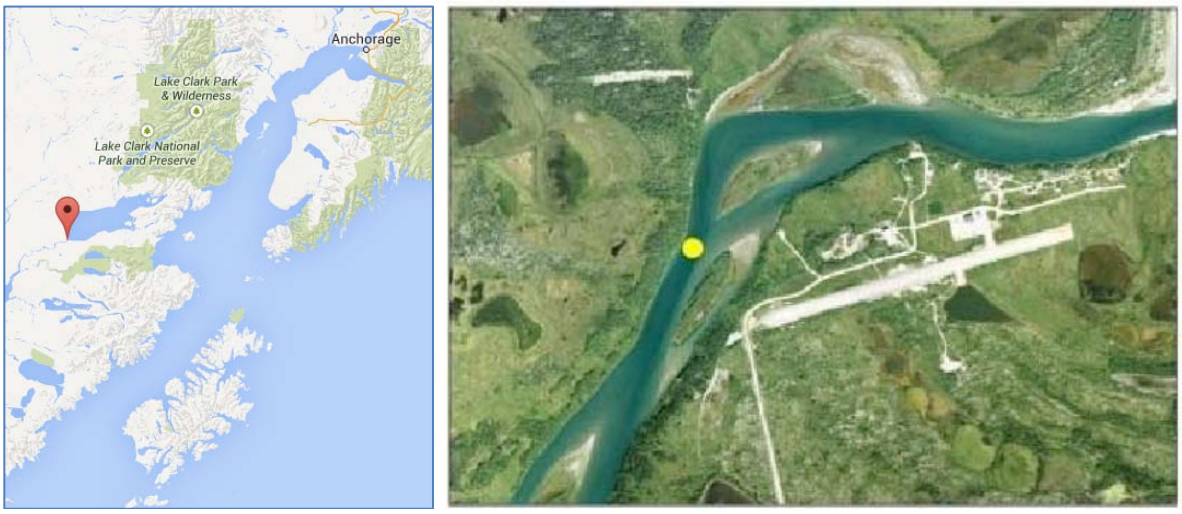

Figure 19: Cook Inlet Region (including Anchorage), Alaska, and site detail at Igiugig, Alaska

Inflow velocities were measured upstream of the RivGen® turbine in Iguigig, Alaska, from August 15 to 25, 2014. Measurements were made with six Nortek Aquadopp profilers deployed in a down-looking orientation from surface catamaran platforms.

Locations were recorded at 5 Hz using Qstarz BT-Q1000 receivers, and this information was merged with the velocity measurements in post-processing. Two additional measurements were made. First, a Nortek Vector velocimeter was deployed on a "turbulence torpedo" lowered from a davit at the stern of the skiff to provide high-fidelity turbulence measurements at 16 Hz. Second, a Nortek Signature profiler (provided by Nortek as cost share to the project) was deployed down-looking on a Doppcat and released to freely drift over the turbine and observed flow patterns at 8 Hz. The data return was 100% from all instruments, and the resulting cumulative sampling time (sum of all instruments) is about 300 hours of river velocity data.

The velocity measurements, which vary in space and time, are subject to measurement uncertainties which are predominantly the Doppler noise Δu_n of the instruments. The streamwise flow u, for example, is decomposed as

$$u(x,y,z,t) = \bar{u}(x,y,z) + u'(x,y,z,t) \pm \Delta u_n \pm \Delta u_{sk}$$

where $\bar{u}$ is the mean flow calculated from 10 minutes of data and Δu_n is estimated as a constant noise level of 0.04 m/s for the 2 MHz Aquadopps and 0.01s m/s for the 1 MHz Aquadopps. There are additional uncertainties resulting from imperfect station keeping, measured via GPS as $\Delta u_{sk} \approx 0.1$ m/s.

The space and time variables also have uncertainties,

$$x = x \pm \Delta x_{gps} \pm \Delta x_{bs} \pm \Delta x_{sk}, \qquad t = t \pm \Delta t_{cd},$$

which are the result of GPS errors ($\Delta x_{gps} \approx 5$ m), beam spreading of the down looking Aquadopps ($\Delta x_{bs} \approx 3$ m), imperfect station keeping ($\Delta x_{sk} \approx 5$ m), and clock drift ($\Delta t \approx 1$ s).

$$TI(x,y,z) = \frac{\sqrt{\langle u'(x,y,z,t)^2\rangle - \Delta u_n^2 - \Delta u_{sk}^2}}{\bar{u}(x,y,z)}$$

Where $\langle u'(x,y,z,t)^2\rangle$ indicates an ensemble value over 10 minutes of observations at a particular (x,y) station.

These uncertainties are assumed to be uncorrelated and averaging of results significantly reduces the uncertainty, such that robust estimates of the mean flow $\bar{u}(x, y, z)$ at a given position are repeatable. However, spatial gradients of the mean flow will be smoothed over scales finer than the uncertainties Δx. Beyond the mean estimates, robust estimates of the turbulence intensity *TI* are possible if the additional sources of variance from uncertainties are removed following *Thomson et al.* (2012)

3.4.2.1 Field Measurement Results

The river velocity measurements show robust spatial pattern in the mean streamwise flow $\bar{u}(x,y,z)$, with random turbulent fluctuations in time that are approximately $TI \approx 10\%$ of the mean flow at any given location. Figure 3 shows all the $\bar{u}$ observations collected with the Doppcats over 10 days. The temporal and spatial variations are separated by binning individual 10-minute ensembles into 5-m resolution grid cells.

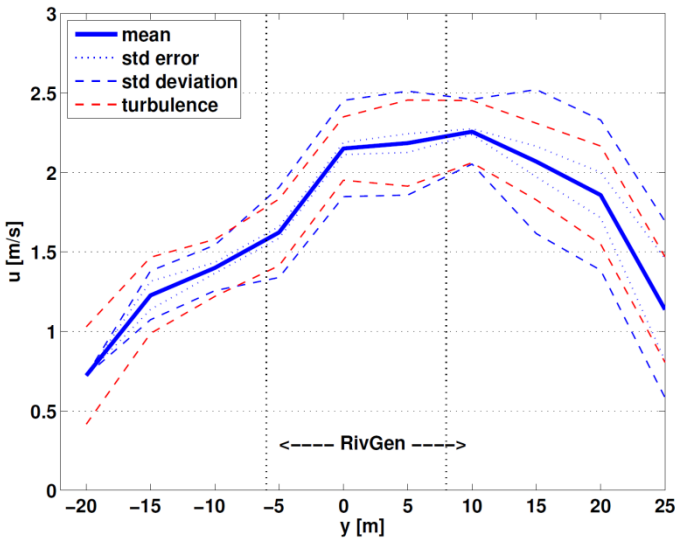

Figure 20: Lateral shear shown as the streamwise flow *u* versus cross-river dimension *y*. Results are the average from 338 stations lasting at least 10 minutes each, collected at positions immediately upstream of the turbine (−20 < *x* < 0 m). The blue dotted line is the standard error in determining the mean flow at each *y*. The blue dashed line is the standard deviation of individual stations. The red dashed line is variation expected from the measured turbulence intensity. The RivGen® turbine cross-section is shown as a black line (−6 < *y* < 8) m.

Variations in the mean flow are extreme, and in many cases the uncertainty in position Δx is a greater source of velocity changes than the $TI \approx 10\%$ turbulence intensity at any given point.

3.4.2.2 Lateral shear results

The lateral shear of inflow velocities across the turbine (i.e., from port to starboard) is the most striking spatial pattern. As shown in Figure 22, the mean inflow velocity varies from 1.6 m/s at the port side of the turbine (y = −6 m) to 2.3 m/s at the starboard side of the turbine (y = 8 m). This 44% increase in speed is a 200% increase in the power density of the flow and likely has profound impacts on the performance of the turbine. This mean flow pattern is robust, as shown by the standard error lines in Figure 22. However the individual ensembles have significant scatter, as by the standard deviation lines in Figure 22. In fact, the standard deviations obtained from the uncertainties in spatial binning are similar, and generally exceed, the velocity fluctuations attributed to turbulence within each ensemble.

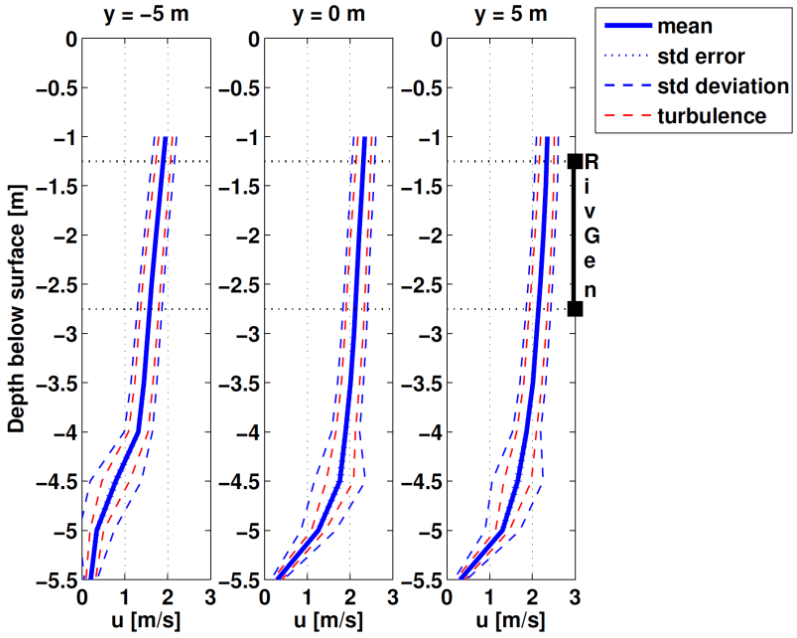

Figure 21: Vertical shear shown as the streamwise flow *u* versus depth below the surface at three positions in the cross-river direction: nominally turbine port (*y* = −5 m), turbine center (*y* = 0 m) and turbine starboard (*y* = +5 m). Results are the average from 338 stations lasting at least 10 minutes each, collected at positions immediately upstream of the turbine (−20 < *x* < 0 m). The blue dotted line is the standard error in determining the mean flow at each *y*. The blue dashed line is the standard deviation of individual stations. The red dashed line is variation expected from the measured turbulence intensity. The RivGen® rotor sweep is shown as a black line (−2.75 < *z* < −1.25 m).

The observed shear is expected given the proximity to a river bend and the ADCP surveys complete the previous year by TerraSond. It appears that deployment of the RivGen® turbine a few meters farther east, at approximately 0 < y < 12 m, would have provided a much more uniform inflow condition. Although a few meters may seem an extreme sensitivity in a river that is 150 m wide, the deep region near the river bend is a much smaller feature and clearly controls the flow.

3.4.2.3 Vertical Shear Results

There is minimal vertical shear in the streamwise inflow velocities upstream of the turbine. As shown in Figure 5, RivGen® is sufficiently far above the riverbed and sufficiently small in diameter relative to the river depth that vertical variations are typically less than 10% of the mean flow value at hub height $z = -2$ m below the surface. Vertical shear is assessed at three locations in cross-river dimension y, nominally turbine port ($y = -5$ m), turbine center ($y = 0$ m) and turbine starboard ($y = +5$m). The pattern from these three profiles is consistent with the lateral shear result, in which flow is strongest at the starboard side of the turbine and in which spatial uncertainties of exceed turbulent fluctuations.

3.4.2.4 Streamwise variations results

The along stream pattern of the streamwise mean flow shown in Figure 24 is dominated by the presence of the RivGen® turbine and the reduction in flow immediately downstream of the turbine. The reduction in the mean flow is significant, from 2 m/s to 1 m/s, and is consistent with momentum deficit expected from energy extraction.

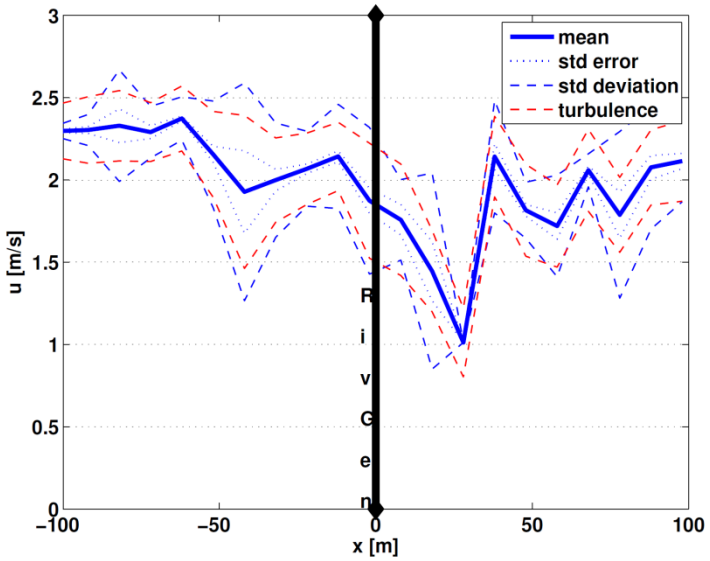

Figure 22: Streamwise flow u upstream and downstream of the turbine ($-6 < y < 8$ m). Results are the average from 563 stations lasting at least 10 minutes each. The blue dotted line is the standard error in determining the mean flow at each y. The blue dashed line is the standard deviation of individual stations. The red dashed line is variation expected from the measured turbulence intensity. The turbine location is shown by the black line ($x = 0$ m).

3.4.2.5 Turbulence spectra and coherence findings

The temporal variability in the velocity components for a given location is shown in Figure 25as the turbulent kinetic energy (TKE) spectra upstream ($x \approx -75$ m) and downstream ($x \approx 50$ m) of the turbine. Spectral are calculated using 10-minutes of motion-corrected velocity data from a Nortek Vector mounted on a 'turbulence torpedo' hanging from a davit at turbine hub height ($z = -2$ m). Motion-compensated spectra have been demonstrated by *Thomson et al.* (2013); *Kilcher et al.* (2014), and the methods herein are the same. The corrections are minor, because the 'turbulence

torpedo' is fared and does not introduce much motion. Spectra are similar up and downstream of the turbine, other than some elevation in the *v* component at mid-frequencies. This is most likely because the downstream measurement was beyond the region of significant wake.

The spectra of all components show an expected $f^{5/3}$ power law at high frequencies, consistent with the isotropic cascade of energy from large scales to small scales through the inertial range.

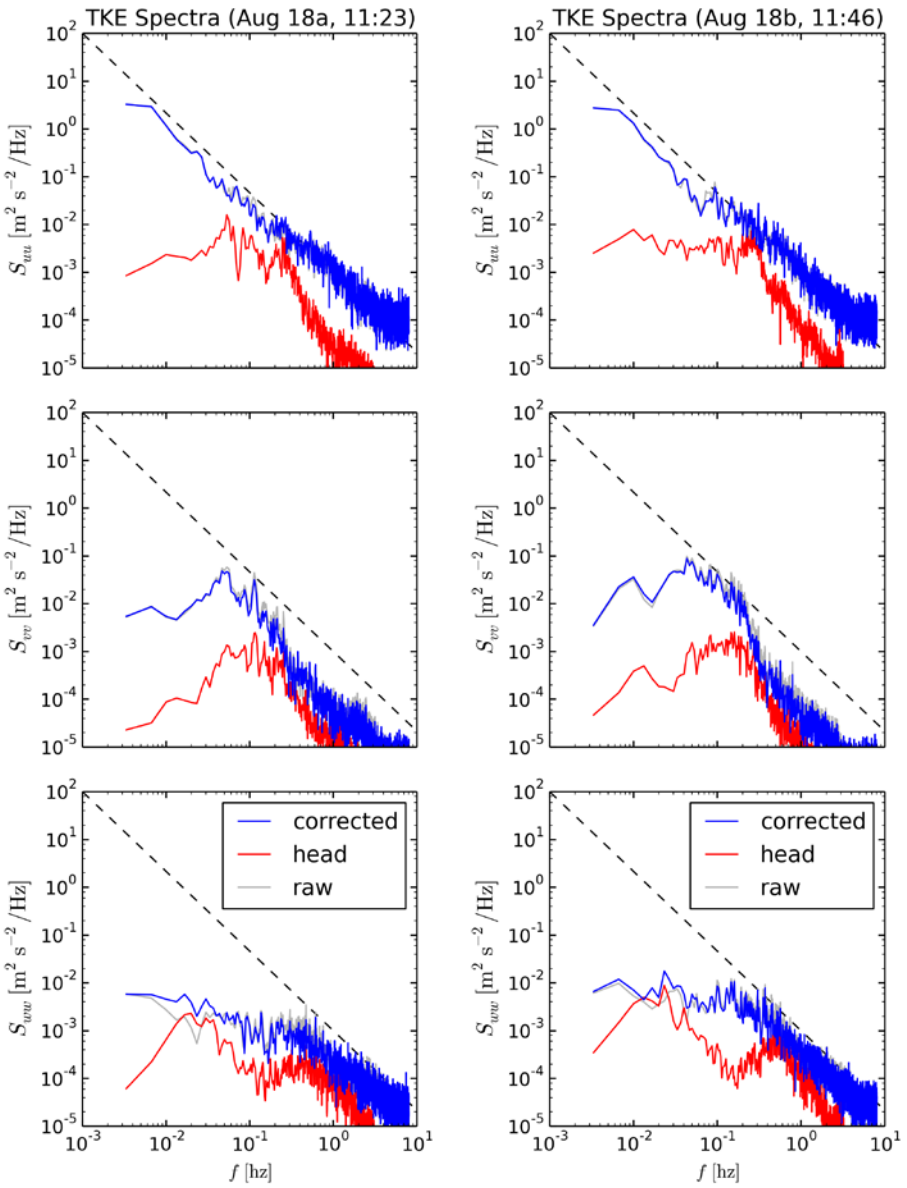

Figure 23: Turbulent kinetic energy spectra density versus frequency for the different velocity components (top is *u*, middle is *v*, bottom is *w*) measured upstream (left) and downstream (right) of the turbine. Corrected spectra (blue lines) use the motion of the instrument head (red) to remove motion from the raw spectra (grey lines). Spectral are calculated using 10-minutes of motion-corrected velocity data from a Nortek Vector mounted on a 'turbulence torpedo' hanging from a davit at turbine hub height (z = –2 m).

At lower frequencies, the u components continue the power law, but the v and w components have maxima at $f \approx 0.06$ Hz and $f \approx 0.2$ Hz, respectively. Assuming that the eddies are 'frozen' as they advect with the mean flow (i.e., Taylor's hypothesis), time and length scales are related as

$$2\pi l = \frac{\bar{u}}{f}$$

where f is the cyclic frequency in a TKE spectrum. Thus, the length scales of the maxima in v and w are $l_V \approx 6$ m and $l_W \approx 2$ m. These length scales are consistent with the expectation that the 6 to 7 m depth of the main river channel limits the scale of 3D isotropic turbulence and that vertical motions w are further limited by the distance from the measurement volume to the nearest boundary (here, the surface, which is 2 m away).

More puzzling is the lack of maxima in the u component spectra, which would be expected to be similar to the v component. This may be related to leakage at low frequencies, where subtle changes in station keeping of the boat against the river flow may add additional variance. Alternatively, the low frequency energy in the u component could be contaminated by deviations from the frozen field approximation, which are expected for the large scales that take a relatively long time (> 10 s) to advect past the instrument. Although the physical reason and relation to $f^{-5/3}$ is unclear, the empirical result is useful: the temporal variations in the flow are dominated by large fluctuations over long time scales (> 10 s).

The turbulence spectrum is equivalent to the lagged auto-correlation of a given velocity time series. Figure 26 shows this calculation for a Doppcat measurement upstream of the turbine, as well as the lagged correlation *between* two simultaneous Doppcat measurements separated by 10 m in x. Consistent with the upstream TKE spectrum, the auto-correlation result shows significant correlations on time lags of up to ±40 s. The correlation between two simultaneous independent measurements shows almost an identical result. This is contrary to the expectation of a distinct, sign-definite lag between the two measurements, as would be expected if the flow was truly a frozen signal advecting along or was wave-like. Such a flow would be the ideal case for implementing feed-forward control in a turbine, because an upstream measurement could be projected to the turbine with a known time lag.

Despite the general lack of coherent lags in simultaneous flow measurements at various separation distances (other examples are similar to Figure 8), the inflow at the site RivGen® is still amenable to control strategies. The streamwise flow appears to be coherent at large space and time scales. On short space and time scales (i.e., small eddies), the turbulence likely evolves too quickly to observe lags, and on longer time scales the lags are essentially zero for separations of O(10 m). The zero lag result dominates because the longer scales contain the most energy. Thus, at any individual fixed point, such as the turbine location, the most robust preview of the flow would be the previous 10 to 30 s of flow *at that location*. An upstream measurement would have no increased skill relative to this self-forecast, because the only thing different at the upstream measurement location would be the small, incoherent eddies. Restated: the large velocity fluctuations tend to last at least 10 s, and on those time scales localized measurements are equivalent to any upstream measurement. (This is akin to the famous 'dummy' forecast in meteorology: synoptic weather patterns last longer than one day, and thus a simple forecast that tomorrow's weather will be like today's weather is quite skillful.)

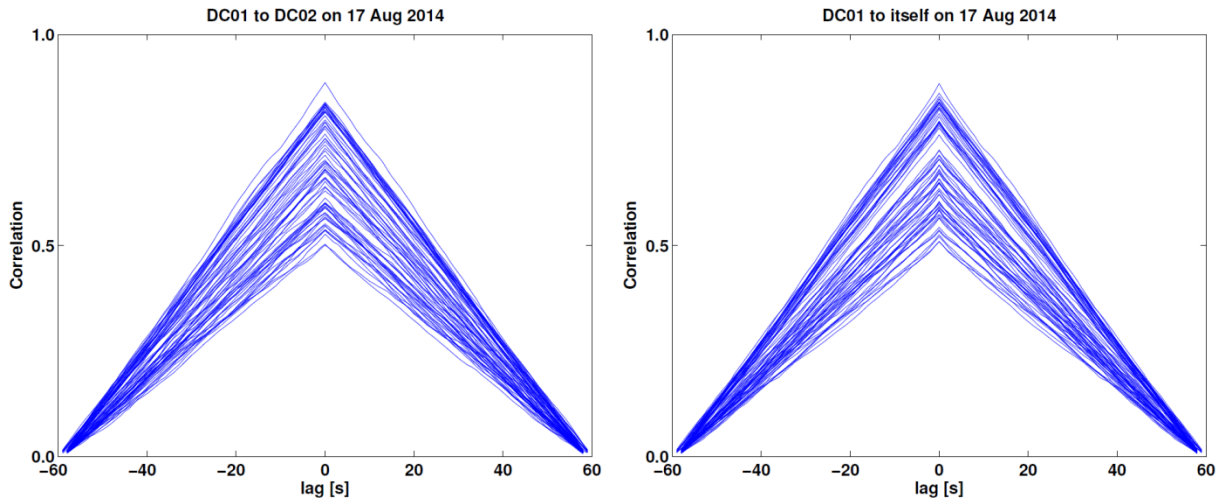

Figure 24: Lagged correlations between two upstream Doppcat velocity measurements separated by 10 m (left) and the same calculation for single Doppcat measurement (right). Correlations are calculated using raw velocity data (1 Hz) in one-minute ensembles, after correction for platform motion using the GPS data.

At this site, and likely at many other river sites, flow is generally steady at a given location, but flow varies dramatically between locations, particularly across the river. The primary result here is that 1) a lateral change in position of a few meters results in changes to flow speed that far exceed the turbulence fluctuations at any given location and 2) the turbulence is dominated by long time scales. Simply put, this is a site for which it is more important to know where you are than to know what time it is.

3.4.3 Problems Encountered and Departure from Planned Methodology

The field measurement campaign progress smoothly and data recovery was excellent. This is a testament to the competence of the measurement teams from University of Washington and NREL.

3.4.4 Assessment of Their Impact on the Project Results

No impact.

3.5 Control System Implementation and Verification

3.5.1 Original Hypotheses

ORPC will implement the feedforward control scheme on RivGen® and collect data to verify the projected increases in energy generation.

Using the analytical results provided from simulation and data analyzed, project the increases in System Performance Advancement (SPA) values.

Provided that the stage gate is satisfied, feedforward control will be implemented on an ORPC TGU. This will likely require additional Doppler instrumentation to be installed on the TGU and the optimal feedforward controller (Task 2.0) implemented in hardware on either the TGU or shore control station.

Validation will involve operating the TGU for a 30 day period. For 6 hour time slots within this period, feedback or feedforward control will be randomly selected.

As part of this task the following items will be provided:

- Develop test plan for validation of control schemes in a RivGen® deployment.
  - Test plan will elucidate methodology for evaluating differences between baseline and proposed control schemes.
  - Test plan will elucidate methodology for reducing uncertainty in $C_P - \lambda$ curves, through a combination of real-time inflow monitoring and before/after deployment comparisons of the flow field around the RivGen® turbine.

The energy loss metric (E_{loss}), representing the difference between optimal and actual power capture, will be calculated for control schemes described in field test plan. This will enable a direct quantification of the power enhancement afforded by feedforward control, confirm that changes in the component performance metrics are directly attributable to changes in the control scheme, and verify that the targeted increases in component performance metrics have been attained.

3.5.2 Approaches Used

3.5.2.1 Overview of RivGen® Power System

The RivGen® Power System consists of a turbine generator unit (TGU) that rests on a pontoon structure that in turn sits directly on the river bed when submerged. The 2015 version of the system has modifications to reduce towing loads on the river surface, which increase hull speed; increased pontoon lengths to increase hull speed, and to provide additional buoyancy; and a fairing added to the chassis to increase turbine capture area. Other changes made to instrumentation and controls are outlined below.

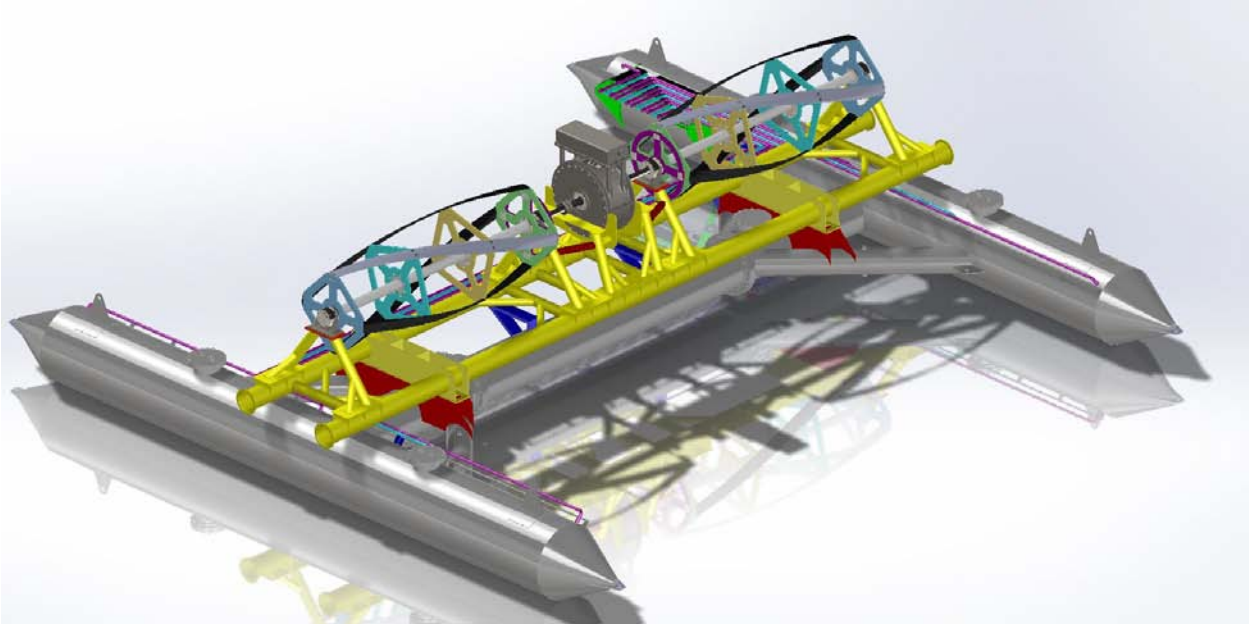

Figure 25: Schematic of 2014 RivGen® Power System.

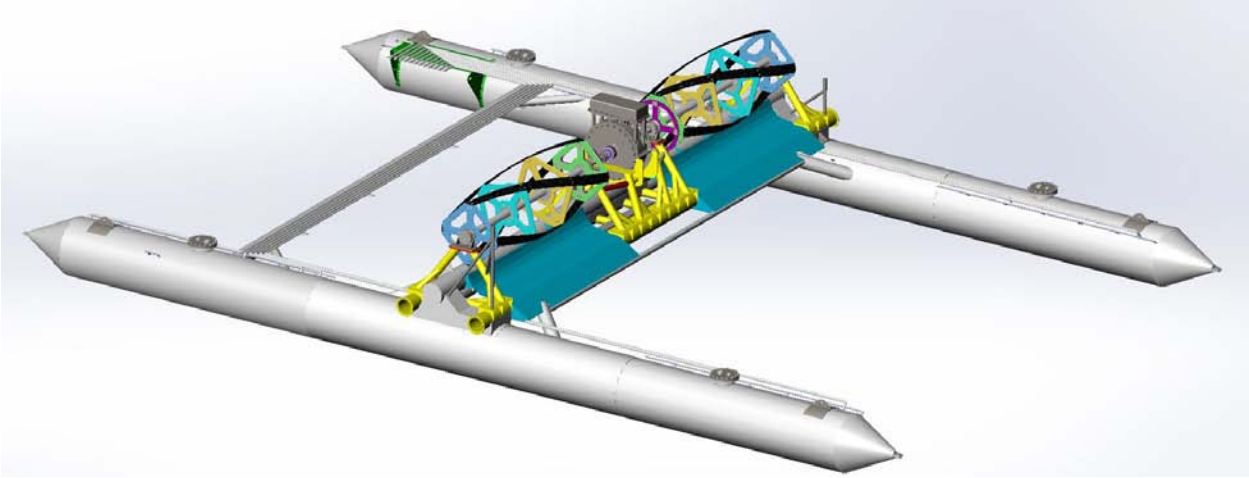

Figure 26: Schematic of 2015 RivGen® Power System, showing detail of fairing beneath TGU and longer pontoons. Turbines and generator are identical to 2014 model.

The RivGen® Power System has the same operating principles and design characteristics as the TidGen® turbine but is intended for deployment in shallow river sites only, due to its smaller cross sectional area, and pontoon support structure.

This RivGen® TGU (without fairing) was tested in Eastport, Maine in 2012 and 2014, and the full power system, including pontoon deployment system, without fairing, was deployed in Igiugig, Alaska in 2014, and with fairing in 2015. Testing in Maine focused on ensuring functionality and reliability of the system prior to delivery to Alaska. In the Maine trials, electrical transmission mirrored that of the TidGen® turbine, where AC voltage provided by the generator was converted to boosted DC voltage subsea in an

adjacent power electronics module. This proved to be functional but had drawbacks in that the majority of power electronics were located subsea so that in the event of an electrical failure it would be cost- and schedule-prohibitive to fix. It was decided to move the AC/DC conversion from subsea to the on shore station in Igiugig, making all power electronics field serviceable. This also meant that the control loop for the generator output moved from the subsea power electronics module to a shore station PLC.

3.5.2.2 Mechanical system

Over the winter of 2014-2015, several improvements were designed for, and implemented on the RivGen® device, including changes to enhance efficiency, ease of deployment, and structural integrity.

One of the unexpected challenges encountered during the 2014 RivGen® deployment was that the RivGen® device could not be towed to its mooring system. A cross member that ran cross-stream between the two pontoons resulted in a large drag load and low hull speed. Analysis of the towing capacity of various arrangements was conducted to determine how to modify the unit to reduce drag. This analysis showed that the removal of the cross section would result in a system that could be towed/pushed more easily than the Flexifloat barge used for general river operations. Additional buoyancy would also reduce drag forces and increase hull speed, and the most effective best way to increase buoyancy was to add length to the main pontoons.

Because the cross sectional member was an important structural element, its removal required additional structural supports for the chassis, a new interface between the pontoons and the chassis, and new routing for air and water pipes between the pontoons. A primary concern of removing the structural cross member was maintaining or increasing overall system stiffness. To ensure the device's strength and stiffness would not be compromised by the removal of the cross-member, finite element analysis (FEA) of the device under the loads predicted by the 2D computational fluid dynamics (CFD) was conducted. Part of the required structural stiffness was provided by the fairing added in 2015 to shape the flow into the turbine. This addition was primarily designed to increase system efficiency, but had structural benefits also.

Pontoons were extended to increase buoyancy and hull speed.

These changes were implemented in Nikiski, Alaska and system assembly was completed in the field in Igiugig, Alaska.

3.5.2.3 Electrical system

The RivGen® Power System uses a direct drive permanent magnet generator, also referred to as a permanent magnet synchronous generator (PMSG) to generate electricity. PMSG has the advantage of higher efficiency and reliability. Because of its lack of a field winding, a PMSG is typically controlled by a series of power converters.

The RivGen® generator has a maximum output rating of 50kW. The stator consists of 3 sets of windings with each phase wound around 18 stator poles. Such a system will generate 3 Phase AC voltage with voltage amplitudes and frequency directly proportional to generator RPM. Generator electrical frequency will be at 18 times the turbine rotor frequency. Generator current is also alternating and its magnitude will be proportional (to a first order) to the mechanical torque applied by the turbines. The RivGen® generator originally used rectification circuitry inside a subsea enclosure to convert three phase AC power from generator into DC power. The enclosure had additional electronics to boost the DC

voltage through active boost circuitry. This is the same implementation as for the TidGen® generator. For the 2015 field testing this component was moved to shore to improve accessibility and serviceability.

The single line diagram for the 2015 test is shown in Figure 27.

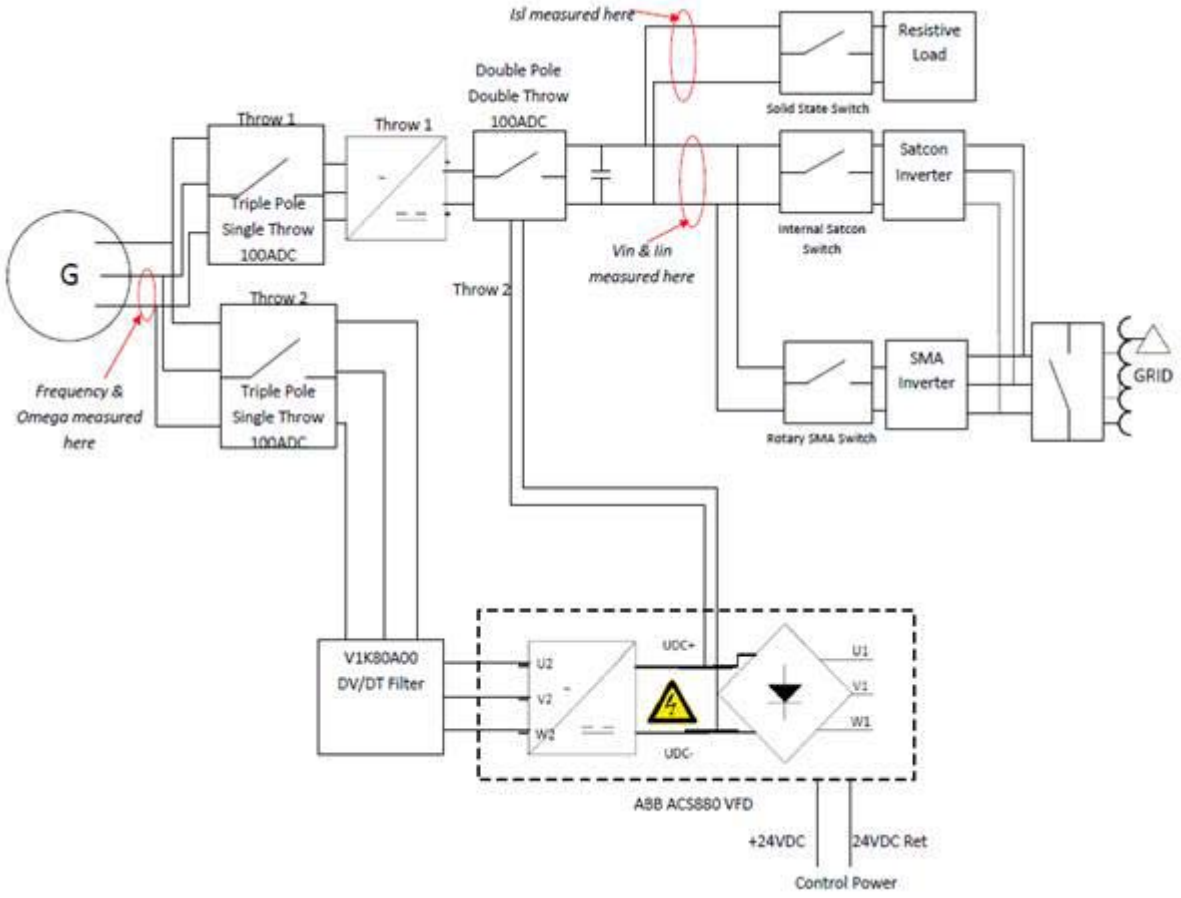

Figure 27: 2015 Igiugig shore station electrical system architecture

3.5.2.4 Power dissipation

The shore station was designed to be capable of operating the RivGen® turbine through two different rectifiers, two different inverters, and supplying power to two different loads. Because of grid connection difficulties in 2014, it was deemed prudent to have several different means of grid connection on site, with the major point of redundancy being the availability of a SMA 20kW PV inverter and a Satcon PowerGate 50kW PV inverter. Both inverters were tested during prior dynamometer tests and both were functional with the RivGen® generator, although the Satcon inverter was limited with a narrow voltage range, and the SMA inverter was unable to accept external controller commands.

In addition to the inverters, the system featured a secondary DC load bank capable of dissipating power from the RivGen® TGU through a DC load bank enable control and testing of the RivGen® without exporting power to the Igiugig grid. A UPS system allows use of this secondary load to stall the turbine and shut it down should grid power fail in Igiugig.

3.5.2.5 Igiugig Grid

The Igiugig grid is diesel electric generator (DEG) microgrid typical of Alaskan villages. Three 65kW diesel generators are available, although at any one time only one or two of the generators are providing power. Transmission voltage is 3 phase, 480V. Power quality and voltage are maintained by Diesels. Small wind turbines (several Skystreams and a HAWT wind farm) are connected to the grid, but provide negligible power. Figure 35 shows the average monthly load in Igiugig over a 3.5 year period. As this graph shows, there is nearly a large variation from lowest to highest load levels over the course of a year, with peak demand in the winter months.

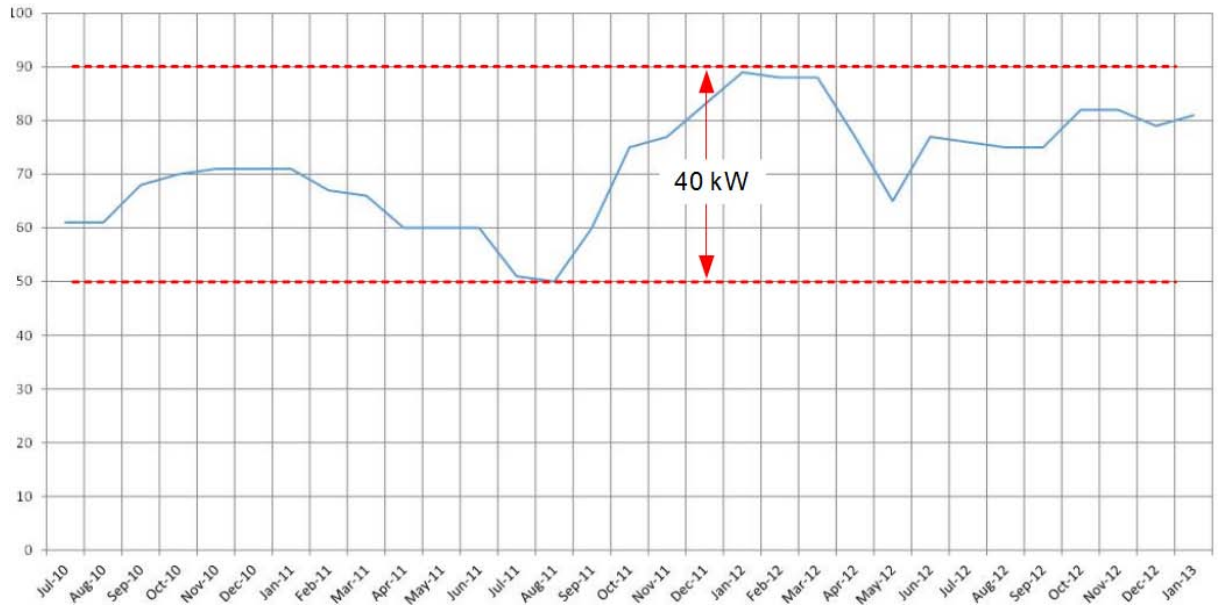

Figure 28: Monthly average load in Igiugig from July 2010 to January 2013

Figure 36 shows the variation in 15 minute load over a single 24 hour day. As this chart highlights there can be nearly a large variation in load over the course of a single day. This chart will not capture true load peaks due to the 15 minute sample period.

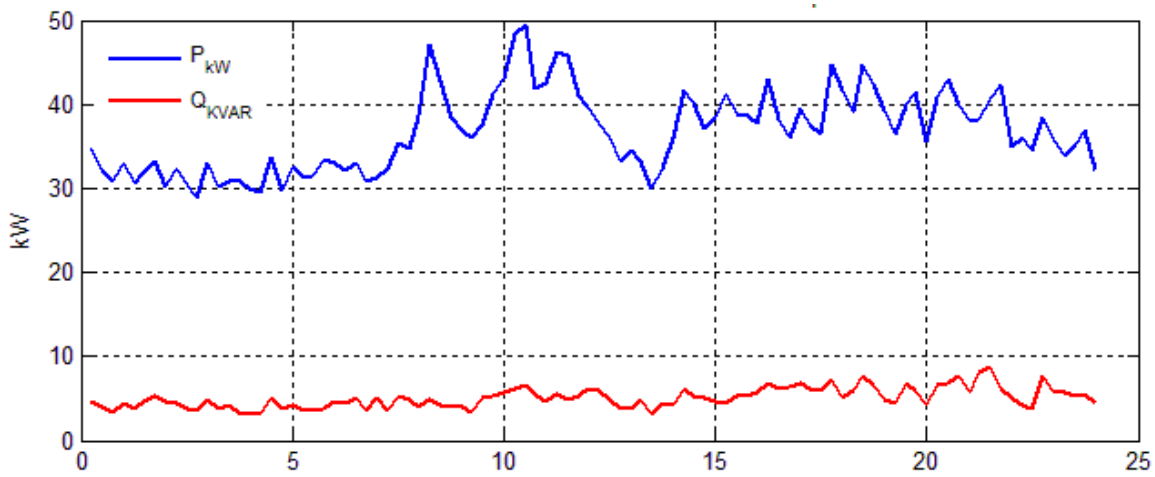

Figure 29: Variation in Igiugig load over 24 hour period note data acquired at 15 minute intervals

Figure 37 gives a representative fluctuation in frequency over the same 24 hour time period. The grid in Igiugig is modern and has fairly low variations in frequency. This chart will not capture true load peaks due to the 15 minute sample period.

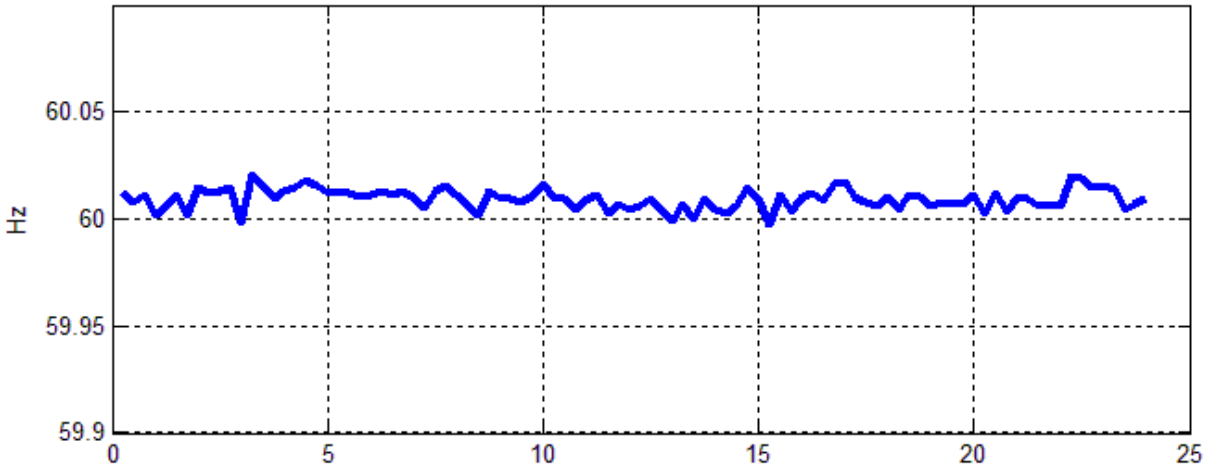

Figure 30: Variation in grid frequency in Igiugig over 24 hour period note data acquired at 15 minute intervals

3.5.2.6 Deployment of TGU and grid connection

Following the device assembly, various systems tests, including on-device instrumentation, turbine brake tests, and buoyancy system tests were conducted to verify functionality before moving the device to the water.

Once the device was secured on its mooring system, power and data cables were installed to shore along with the cables for the cameras that monitored for fish activity around the device

Following final system tests, the RivGen® device was submerged using the modified Side Pivot Launch technique. Despite operational challenges, the deployment of the RivGen® device to the river bottom went well and proved to be a controlled process consistent with model predictions. This proved to be an important validation of the modeling tools in conjunction with 2D CFD loads as a means of establishing conservative simulations for deployment operations.

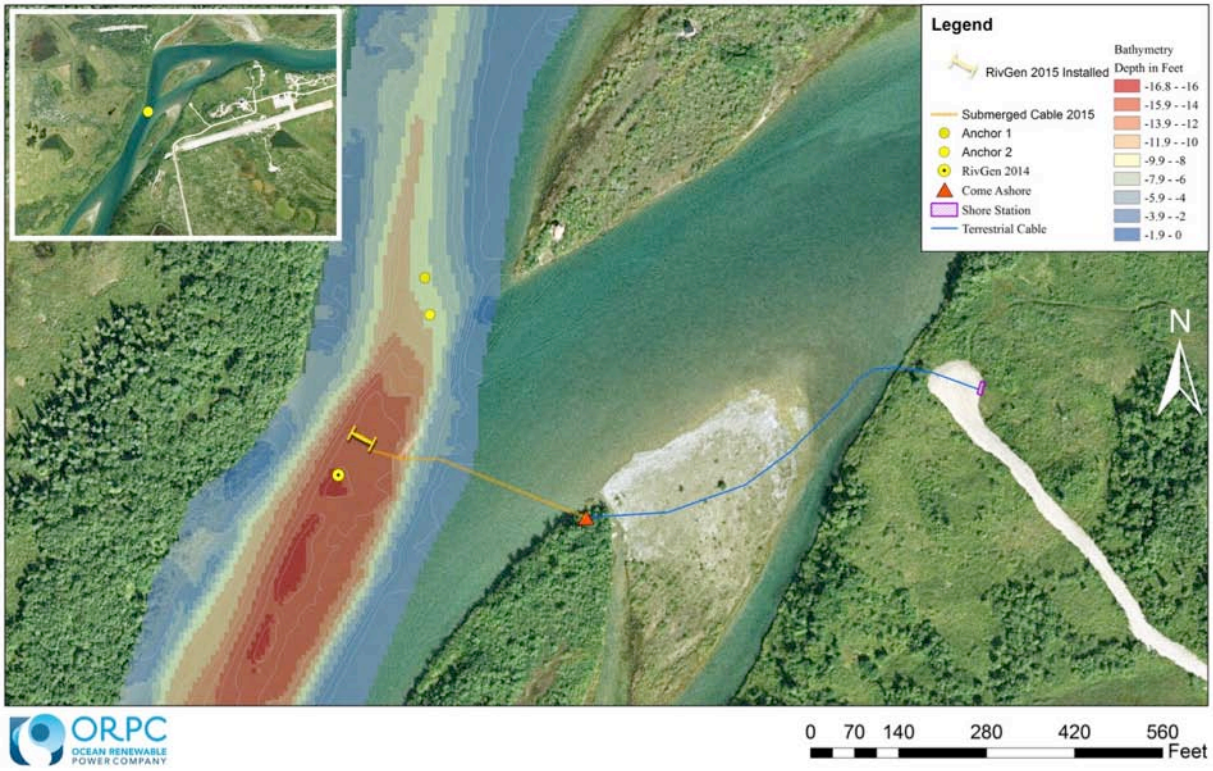

Figure 31: Location of anchors and RivGen® TGU, Power and data cable and shore station, used for 2015 installation. Position is not identical to location of 2014 deployment.

The turbine was deployed adjacent to a bend in the river, which created a strong lateral shear in the streamwise flow as shown in Figure 42. The maximum observed flow velocity in the river was 2.3 m/s, occurring mid-channel, immediately upstream of the turbine. Velocities were reduced to approximately 1 m/s near either river bank.

The ambient turbulence was measured at approximately 10% using Doppler instruments (Thomson et al., 2012) at multiple locations upstream of the turbine. Thus, a typical temporal fluctuation of the inflow velocity is 0.23 m/s above (or below) the time-mean inflow of 2.3 m/s. The 10% estimate was consistent from both Acoustic Doppler Velocimeters (point measurements) hanging at the depth of the turbine using the davit of a small vessel and from Acoustic Doppler Current Profilers pinging downward from surface platforms held on station by a small vessel. The time scale used for the mean calculation is 10 minutes.

The turbulent kinetic energy spectrum decomposes the turbulent fluctuations by the frequency of occurrence. The ambient turbulence in the river was dominated by low frequencies ($f < 0.1$ Hz), as shown in the example included as part of Figure 1. Thus, the fluctuations of 0.23 m/s occur slowly, over 10 s or longer, rather than rapidly. This is especially true for the largest velocity fluctuations. Furthermore, Figure 1 shows that the RivGen® turbine does not respond to rapid fluctuations and these large, slow fluctuations are effectively changes in the “mean flow” that the turbine, and any control algorithm, can respond to in real-time (i.e., without preview information).

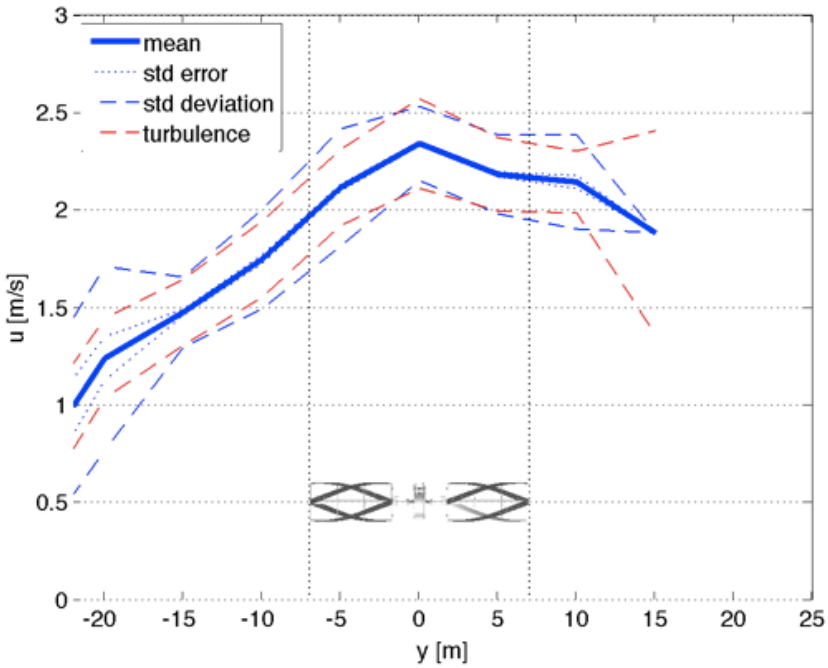

Figure 32: Characteristic inflow shear across the RivGen® turbine. The turbine position is centered at y=0m. The turbulence lines are the temporal fluctuations. The standard deviation lines are the spatial errors associated with the station-keeping method used to collect these data.

Final commissioning tests of the Power Electronics System were completed. This included successful integration of power from the RivGen® device into the Igiugig grid utilizing both the Satcon and SMA inverters. In each case ORPC was able to exercise control of the RivGen® device utilizing different control algorithms with each inverter. Throughout these operations the SCADA system provided reliable data acquisition from the necessary sensors. At this stage of operations the VFD was not available on site due to ordering delays.

Power System operations began on July 20, 2015. The Power System was characterized and performance was compared to 2014 prototype testing. The addition of the fairing showed a 35% increase in power production. The fairing also had the effect of shifting the efficiency curve towards higher tip speeds. Because the turbines are producing power at faster rotational rates they are able to produce peak power further away from the stall point of the turbines, resulting in less down-time due to stall. These results successfully validate that the incorporation of the fairing system leads to the significant gains in power production required to make a power system for remote communities, even those residing on rivers with slower currents, a reality.

During these tests ORPC was able to achieve a relatively consistent 30% penetration into the Igiugig grid that peaked during the evenings near 50% (Figure 45). Output from the RivGen® varied depending on the control scheme being exercised from 10-19 kW.

Over the course of the 2015 operations the RivGen® Power System logged a total of 382 hours of operations producing over 2 MWhrs of power delivered to the Igiugig grid.

Figure 33: Installing the RivGen® device onto its mooring system, Igiugig, AK, 2015

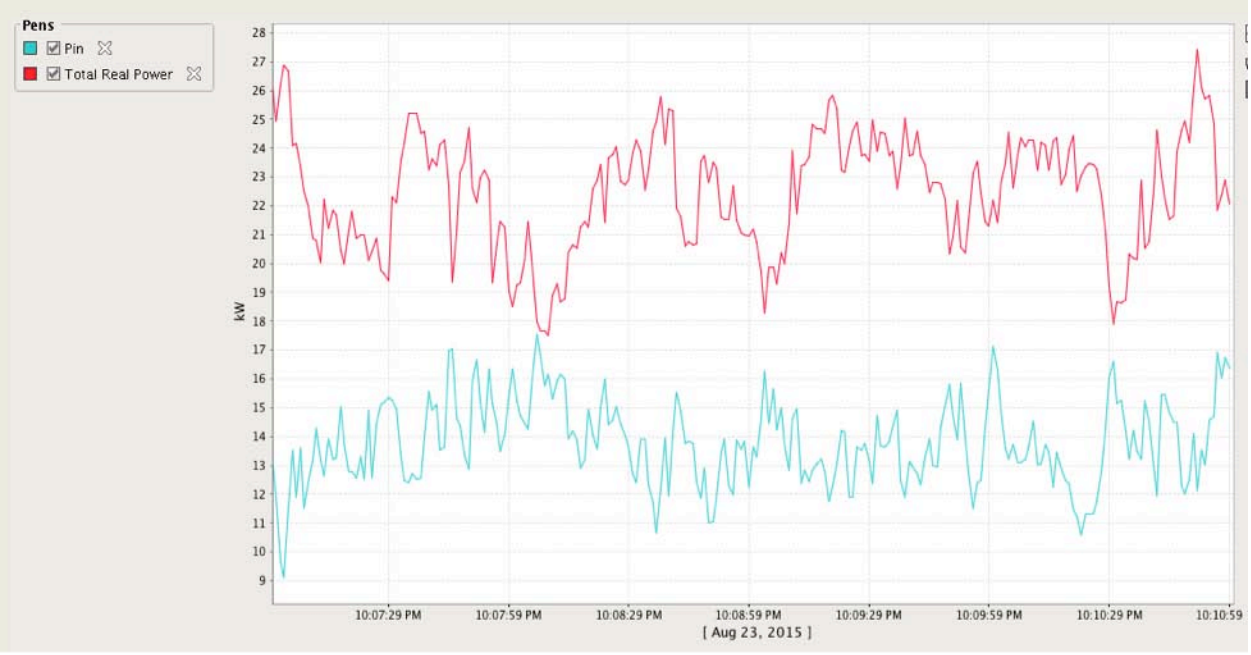

Figure 34: Output from the RivGen® Power System (blue) as compared to the Igiugig load supplied by the diesel generators (red) showing peak of 50% penetration around 10:08 pm on August 23, 2015

During the 2015 deployment season LGL Alaska Research Associates Inc. (LGL) performed a fish monitoring study in compliance with and Alaska Department of Fish and Game fisheries habitat permit for the project. The study collected data from 5 video cameras mounted on the RivGen® device. LGL collected video data for a total of 415 hours, 240 hours during which the RivGen® was in operation. Continuous video footage was collected through the last week of July during the latter half of the peak of the adult sockeye salmon migration. During this time 1.5 million sockeye salmon migrated upstream past the turbine. After this time period 50% video coverage of RivGen® operations was maintained. During the season LGL reviewed 10% of 179 one-hour blocks of footage (6 minutes on the hour) and documented a total of over 1200 fish in the vicinity of the RivGen® device, including over 800 salmon smolt and over 350 adult salmon. No evidence of adverse effects including passage delay by upstream migrating salmon was noted.

On August 18th, 2015, ORPC began retrofitting the shore station to include the VFD drive as part of the power dissipation circuit. During commission of the VFD several wiring issues were noted, including mis-wiring of the VFD input terminals and mis-wiring of the VFD outputs. Upon operation of the Power System the turbine was put into no-load operation. Multiple times during the commissioning events operators applied the electrical brake to the system, leading to rapid braking of the system.

3.5.2.7 Retrieval and removal

On October 1, ORPC successfully completed the decommissioning of the 2015 RivGen® Project. The entire RivGen® Power System is now secured for winter storage in Homer Alaska.

Figure 35: RivGen® TGU loaded on trailer in Igiugig and ready for transport to Homer on September 29, 2015

3.5.2.8 Plant Model Development

To develop a feedforward control implementation, knowledge of the plant must be obtained. We discuss how the plant model was developed.

The moment of inertia (J) for RivGen® was calculated from a CAD model. Based on the experimental agreement between the CAD model and in-water acceleration tests, this value is likely accurate. By pairing steady-state data sets taken at near-zero control torque but sufficiently low tip speed ratio so as to estimate hydrodynamic forcing, an estimate of B can be determined. For these estimates, the inflow velocity was assumed constant and an estimate of generator efficiency of 90% was used to determine $C_p(\lambda)$ from known $\eta(\lambda)$. For two events at distinct control torques, the dynamic equations are

$$J\frac{d\omega_1}{dt} = \frac{1}{2}\frac{\rho A C_{p1} U_\infty{}^3}{\omega_1} - \omega_1 B - \tau_{c1}$$

$$J\frac{d\omega_2}{dt} = \frac{1}{2}\frac{\rho A C_{p2} U_\infty{}^3}{\omega_2} - \omega_2 B - \tau_{c2}.$$

Because torque is not known directly, it is approximated it as a function of current via generator characteristic equation

$$\tau_c = kI$$

where *k* is an unknown constant property of the generator.

From these considerations it follows that an estimate for damping is given by

$$B = \frac{\rho A U_\infty^{\,3}\left(\frac{C_{p2}}{\omega_2} - \frac{I_2 C_{p1}}{I_1 \omega_1}\right)}{2\left(\omega_2 - \frac{I_2 \omega_1}{I_1}\right)}$$

A single estimate of *B* was achieved by averaging the result of all possible pairings of appropriate points.

3.5.2.9 Inflow Characterization

To quantify temporal-spatial variations in the shear profile, two upstream-looking 2-beam Nortek AWAC 400 kHz Doppler sonars were mounted at each end of rotor (Figure 47). The beams were separated by 50° in look-angle, the velocities were sampled at 1 Hz, and the Doppler noise was 0.05 m/s. The AWACs are vertically offset by 1 m to limit cross-talk at the horizontal intersection of the beams.

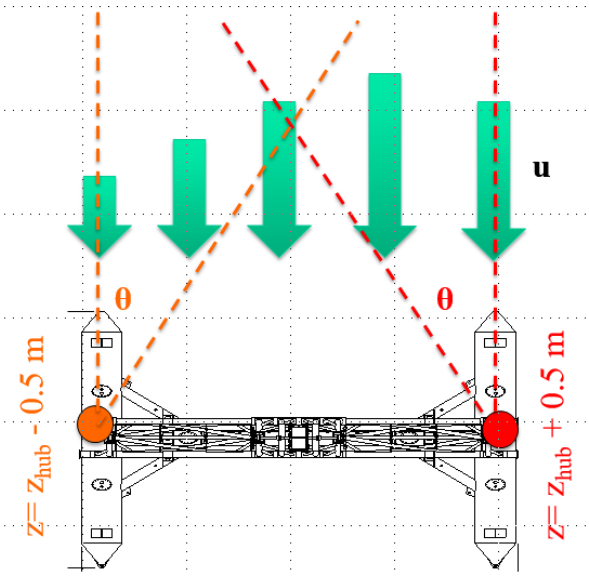

Figure 36: Plan view of RivGen 2015 deployment AWAC strategy. Each AWAC has two beams separated by angle θ=50° shown as orange dashed lines. Crossing beams are separated vertically to reduce cross-talk.

The AWACs record along-beam velocities in ten bins with 2 m resolution and a 1 m blanking distance adjacent to the sonar head. The oblique beams were separated from the upstream-looking beams by angle θ=50°. The spatially-varying profile can be reduced to a single, representative inflow velocity through a bin-weighted average as

$$U_\infty = \frac{\left(\frac{\sum_{i=1}^{10} W_{p1,i} B_{p1,i}}{\sum_{i=1}^{10} W_{p1,i}}\right) + \left(\frac{\sum_{i=1}^{10} W_{s1,i} B_{s1,i}}{\sum_{i=1}^{10} W_{s1,i}}\right) + \left(\frac{\sum_{i=1}^{10} W_{p2,i} B_{p2,i}}{\cos\theta}\right) + \left(\frac{\sum_{i=1}^{10} W_{s2,i} B_{s2,i}}{\cos\theta}\right)}{\sum_{i=1}^{10} W_{p2,i} + \sum_{i=1}^{10} W_{s2,i} + 2}$$

where *W* is a set of weighting vectors for port upstream (*p1*) and oblique beams (*p2*) and starboard upstream (*s1*) and oblique beam (*s2*), and *B* are the along beam velocities in each bin. This method is adaptable to other turbine geometries and can be modified to provide and inflow estimate for either rotor by adjusting the weighting factors. The addition of '2' in the denominator accounts for the fact that the beams sample bins on each edge twice, once by an oblique and once by an upstream looking beam. If points over only one rotor are to be considered, this is replaced by a '1'.

3.5.2.10 Performance Characterization

Once an estimate of the representative inflow velocity has been obtained, turbine performance can be estimated. The RivGen® turbine performance was characterized by stepping the turbine through a series of load settings imposed by resistance elements on the shore station, and by use of constant voltage mode with the SMA inverter. The inflow velocity and, therefore, hydrodynamic torque is approximately constant over this period, so the turbine tip-speed ratio (λ) is as well. The performance curve for this 2015 data set is shown with the 2014 performance curve as Figure 48. There is a 35% improvement over the 2014 performance curve. There are three possible explanations for this:

1. *The spatial averaging approach does not produce a representative inflow velocity and kinetic energy flux for calculation of these quantities*. In other words, if the inflow velocity profile changes, the performance curve changes and is not an invariant estimate for turbine performance. This is unlikely, as the power generated by the RivGen® turbine was 30% higher than in 2014 and, as discussed later in this section, non-dimensional performance was observed to be almost identical when operating with only a single rotor during the latter half of testing in 2015.
2. *The location selected for the 2015 deployment enhanced the performance of the turbine more than in 2014*. Performance of the RivGen® turbine in 2014 was substantially higher than during tow testing in unconfined flow in Eastport, Maine. The most likely explanation for that change is blockage, though the enhancement is most significant than would be expected from analytical and computational research on this topic. The further elevation of efficiency in 2015 and shift to a higher optimal tip-speed ratio is consistent with blockage and may explain some of the increase.
3. *For the 2015 deployment, the RivGen® turbine was equipped with a fairing intended to augment turbine power*. The observed enhancement is consistent with 2D simulations of the turbine.

3.5.2.11 Summary of Controller Performance

This project evaluated four types of controllers:

1. $K\omega^2$ – a nonlinear feedforward controller
2. Adaptive $K\omega^2$ – a nonlinear feedforward controller that requires preview information

3. PI-ω – a linear feedback controller
4. PI-λ – a linear feedback controller that requires preview information

These controllers were tested in simulation, emulation, a laboratory flume, and the field. The adaptive $K\omega^2$ controller performs similarly to the non-adaptive version of the same controller and may be useful in tidal channels where the mean velocity is continually evolving.

Outcomes from testing modalities are summarized in Table 27: Testing modality outcomes. The clear message is that the feedforward $K\omega^2$ controller out-performs the feedback controllers in almost all aspects and modes of evaluation. The conclusions drawn from single modalities of testing are generally shared. In practice, the energy capture differences between controllers (while a substantial improvement over the baseline performance of the TidGen turbine) were minimal in the laboratory and field. Each testing modality also contributed unique information about controller performance, measurement, and implementation.

Table 17: Testing modality outcomes

Outcome	Simulation	Emulation	Laboratory Flume	Field
Energy Capture (E_{loss})	$K\omega^2$ superior (smallest E_{loss})	PI-ω superior (smallest E_{loss})	Minimal difference	Minimal difference
Stability at $\lambda < \lambda^*$	$K\omega^2$ superior (most stable)	-	$K\omega^2$ superior (most stable)	$K\omega^2$ superior (most stable)
Range of Command Torque	$K\omega^2$ superior (smallest range)	-	$K\omega^2$ superior (smallest range)	$K\omega^2$ superior (smallest range)
Range of ω	PI- ω superior (smallest range)	-	PI-ω superior (smallest range)	PI-ω superior (smallest range)
Minimum Update Rate	10 Hz	10 Hz	-	-
Impact of Sensor Noise	Degrades stability	-	Degrades stability	-
Effect of Filtering	Recovers stability	-	Recovers stability	Reduces stability[4]
Unique Insights		Emulation achieves good agreement with field observations	Controller performance unaffected by increased turbulence	- Observations of turbine wake - Potential for large improvement through blockage - New capability to characterize turbines in sheared flow

3.5.2.12 Comparison of Control Evaluation Methods

Each of the methods used to evaluate turbine control (simulation, emulation, laboratory experiments, and field operations) provided insight into control methods. The modes of testing are compared in Table 28. The most notable aspect of testing is that no mode, including field testing of a turbine with a standard suite of instrumentation, is able to investigate all aspects of controller development and

[4] This is reduction in stability is hypothesized to have more to do with the specific filter implementation on hardware than an inherent stability reduction through filtering for a given class of controller.

turbine performance. The combination of modes does, however, allow comprehensive investigation and increases confidence in the conclusion drawn about controller performance.

Table 18: Testing modality summary

Investigation Aspect	Simulation	Emulation	Laboratory Flume	Field
Turbine Performance	Deterministic Cp-λ curve	Deterministic Cp-λ curve	Measured on turbine geometrically similar to RivGen	-
Power Train Performance	Constant efficiency	Measured on hardware similar to RivGen	-	-
System Performance (turbine + power train)	Product of turbine and power train performance	Product of turbine and power train performance	-	Measured on RivGen
Turbine Dynamics (J, B)	Simulation input	Emulation input	Measured	Measured
Stall Events	Deterministic λ limit	Deterministic λ limit	Self-determining	Self-determining
Inflow Velocity	Deterministic point time series	Deterministic point time series	Turbulent flow field	Turbulent flow field
Cost	Low	Moderate	Moderate	High

Simulation was able to establish requirements for minimum controller update rates to maintain stability. The need for control loops to update at a rate 1-2 orders of magnitude faster than perturbations in the flow can pose challenges for commercial-off-the-shelf SCADA systems. If update rates on the order of 10-100 Hz cannot be accommodated by a SCADA, then no controller is likely to perform acceptably. Second, simulation identified a poor estimate of the turbine rotation rate as the most likely explanation of the instability observed in attempting to operate the TidGen turbine at its optimal tip-speed ratio set-point using $K\omega^2$ control. This motivated explorations into filtering methods to provide a controller with a low-noise estimate for this quantity, especially if the primary measurement of this quantity is significantly contaminated by noise. Third, simulation demonstrated that for the RivGen and TidGen turbines, the moment of inertia and damping are low enough for a feedforward $K\omega^2$ controller to optimally harness all energy-containing structures in the flow.

Trends in simulation were largely verified through experiments, which also provided the opportunity to test assumptions about turbine responsiveness and control resilience to varying scales of turbulence. These provided an essential stepping stone between simulation and implementation on a field-scale turbine. Experiments also demonstrated that using “energy loss” as a metric to differentiate between well-designed controllers operating at an optimal tip-speed ratio set-point is difficult, which anticipated the outcome from field experiments. Future laboratory experiments could benefit from modified control algorithms that use a servomotor to provide virtual inertia or damping to better match the time constant of experimental turbines to those in the field.

Emulation of controllers on hardware at University College Cork provided early validation of simulation results for minimum update rates and successfully reproduced the performance of the RivGen turbine

during 2014 field trials. A future project would benefit from the ability to install power train hardware on an emulation test rig and implement control architectures in advance of a field deployment. This would reduce the amount of time required for integration in the field. For this specific project, however, a significant emulation campaign would have required a second dedicated power train and electronics due to the lead times associated with turbine field deployment (i.e., an effective emulation and field campaign could not have both been conducted in 2015 with a single power train). Dynamometer testing had been conducted with the RivGen generator but this testing was a rather limited test intended to prove functionality rather than implement full grid integration emulation. The dynamometer test setup could be expanded to accomplish these studies.

Field testing confirmed trends identified in simulation, emulation, and experiments, but success in the field campaign would not have been likely without these other investigations.

3.5.2.13 Controller Performance Metrics

The metric of "energy loss", the ratio of energy actually harvested by the turbine to the energy that could have been harvested by a turbine operating at maximum efficiency over a period of time was initially proposed a the sole benchmark of controller effectiveness. This metric was able to differentiate between controllers in simulation, but not in the laboratory or the field. However, for turbines with higher moments of rotational inertia or performance curves with sharper roll-offs around their peak efficiency, controller choice could significantly affect power generation in turbulent flow and energy loss might be a distinguishing metric.

To explore situations in which E_{loss} could be a distinguishing feature in the field, a simulations was carried for the RivGen turbine operating in Iguigig under $K\omega^2$ control. In the simulation, the rotational moment of inertia was varied and the performance of curve replaced with a hypothetical "sharper" one in which efficiency decreases more rapidly to either side of optimal tip-speed ratio. Results are summarized in Table 29. Only for a sharper performance curve does E_{loss} significantly degrade as turbine inertia increases. This is because the high-inertia turbines are still able to operate at near-ideal gain levels, such that energy is only "lost" when they are unable to maintain a favorable tip-speed ratio during a turbulent gust. If performance is only a weak function of tip-speed ratio, this "off optimal" performance has little cost. In general, for turbines where performance is a stronger function of tip-speed ratio or are responsive to a wider range of turbulent length scales, the consequences of higher inertia will be more pronounced and E_{loss} could be incrementally reduced through preview control (e.g., adaptive $K\omega^2$ control).

Table 19: Simulated E_{loss} [%] with increasing inertia and sharper performance curve for RivGen Turbine

Moment of Inertia (*J*)	Actual Performance Curve (2015)	"Sharper" Performance Curve
Actual (2778 kg m^2]	3.2	3.2
10x increase	3.5	5.3
100x increase	3.7	6.6

This outcome is also apparent when one considers the ability of different hypothetical versions of RivGen (varying moment of inertia) to harness the energy contained in turbulent flow. With its moment of inertia, RivGen is able to harness the majority of the turbulent energy in the flow. For flows where more energy is present at higher frequencies (smaller length scales), a turbine with a lower moment of

inertia would have greater bandwidth to harness them. Conversely, a turbine with a higher moment of inertia would be expected to "miss" some of the energy in the flow due to a reduced bandwidth. A turbine with this time constant operating in a flow with a wide range of energy-containing turbulence would benefit from preview control.

Given this, several other measures of controller performance were developed and successfully employed across all modalities of development. First, ability of a controller to operate the turbine without stall was a strong point of differentiation between control architectures, as well as the investigation of measurement noise/uncertainty and filtering measures to mitigate these. Second, controllers were moderately differentiated by the statistics of their torque commands (tighter range suggests less stress on power train) and rotational rate (tighter range suggests simpler grid integration). While other metrics could be applied individually to differentiate controller performance in simulation, emulation, or laboratory experiments, those metrics that can be employed across all testing modalities have the greatest value.

3.5.2.14 Improvement over Baseline Controller for TidGen Turbine

During testing in Cobscook Bay, Maine the TidGen turbine generator was actuated by a non-linear $K\omega^2$ controller. The system could not, however, operate stably with $K = K^*$, which reduced the maximum operational efficiency to 80% of peak, even with an update rate of 2000 Hz. The most consistent explanation for this performance limitation is a noisy estimate for the rotation rate being used to calculate the control torque. This could either be addressed through filtering or modifications to bring the calculation of rotation rate more in line with the method used by the VFD in RivGen turbine testing. Based on the results of this project, the latter would yield better performance.

Estimates of the maximum gain fraction that TidGen® could stably operate are consistent from operating experience and simulation at being approximately 0.5K*. Non-dimensionalizing field results from RivGen testing in 2015 and comparing with TidGen expected gains indicates that TidGen® was operating at 80% of its maximum power, and with a 20% ELoss. This is consistent with earlier predictions of TidGen® performance.

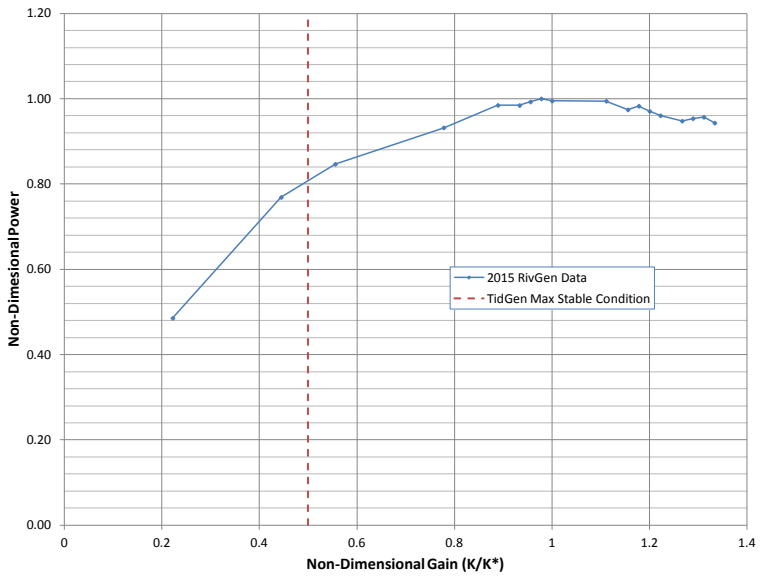

Figure 37: Non-dimensional Power for $K\omega^2$ controller as a function of non-dimensional gain. Test data from RivGen testing in 2015 are plotted, along with an estimate of the maximum stable gain for TidGen operations at

0.5K*. Based on the intersection of the curves, we expect that TidGen was operating at 80% of its maximum power capability.

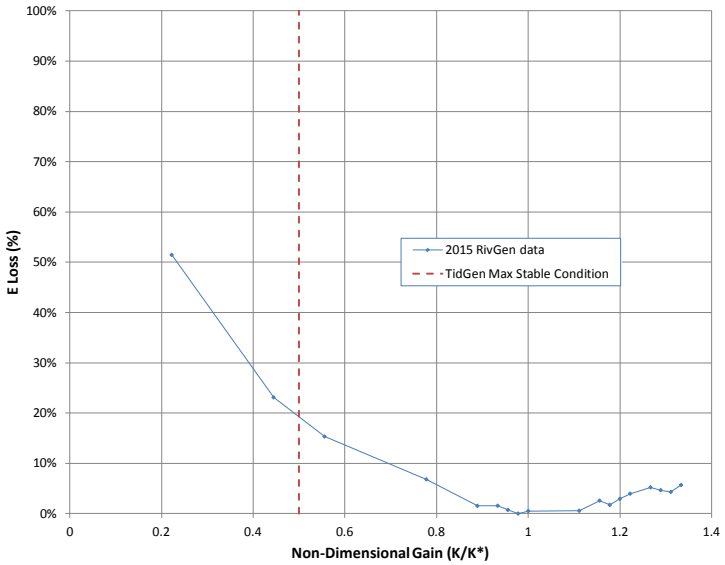

Figure 38: Non-dimensional ELoss for $K\omega^2$ controller as a function of non-dimensional gain. Test data from RivGen testing in 2015 are plotted, along with an estimate of the maximum stable gain for TidGen operations at 0.5K*. Based on the intersection of the curves, we expect that TidGen was operating with an ELoss of 20%.

In a tidal environment, the mean currents will change continually from slack to peak flow. Initially, to maximize power, an adaptive $K\omega^2$ controller might need to be employed if the turbine's efficiency is a function of both velocity tip-speed ratio. Laboratory experiments suggest that a properly tuned adaptive $K\omega^2$ controller can maintain optimal efficiency for a time-varying inflow velocity. Beyond the turbine's rated speed, the control objective would shift from maximum efficiency to maintaining a constant power output. The $K\omega^2$ controller can be used to achieve this by adjusting K to a value away from K^*. This is another form of an adaptive $K\omega^2$ controller. The most stable operation above rated power is achieved by increasing the tip-speed ratio. However, this would require a temporary surge in power if the turbine needed to be brought to a stop while operating above rated speed (the turbine would pass through its maximum power point before a brake could be applied). Power can also be shed by increasing the tip-speed ratio.

3.5.3 Problems encountered and departure from planned methodology

No problems were encountered with development and tracking of LCOE calculations.

3.5.4 Assessment of their impact on the project results

None.

4 Products

4.1 Publications

Cavagnaro, R. (2014, November). Impact of turbulence on the control of a hydrokinetic turbine. Proceedings of the International Conference on Ocean Energy 2014, Halifax, Nova Scotia, CA, November 4-6, 2014.

Cavagnaro, R., Polagye, B., Thomson, J., Fabien, B., Forbush, D., Kilcher, L., Donegan, J., & McEntee, J. (2015, September). Emulation of a hydrokinetic turbine to assess control and grid integration. Presented at 11th European Wave and Tidal Energy Conference, September 6-11, 2015, Nantes, France.

Forbush, D., Cavagnaro, R., Fabien, B., Polagye, B., Donegan, J. & McEntee, J. (2016, April). Development of cross-flow hydrokinetic turbine controller in simulation, experiment, and field testing. Presented at 2016 Marine Energy Technology Symposium, April 25-27, 2016, Washington, DC.

Forbush, D., Polayge, B., Thomson, J., Fabien, B., Donegan, J., & McEntee, J. (2015, April). Characterization and control of cross-flow turbine in shear flow. Proceedings of the 3rd Marine Energy Technology Symposium. April 27-29, 2015, Washington, DC.

Forbush, D., Polagye, B., Thomson, J., Kilcher, L., Donegan, J., & McEntee, J. (2016). Performance characterization of a cross-flow hydrokinetic turbine in sheared inflow. International Journal of Marine Energy (under review).

Guerra, M. & Thomson, J. (2016, April). ORPC RivGen® wake characterization. Presented at Marine Energy Technology Symposium 2016, April 25-27, 2016, Washington, DC.

Guerra, M. & Thomson, J. (2016). Ambient and wake turbulence measurements at marine energy sites from a five beam AD2CP, Ocean Sciences Meeting 2016.

Thomson, J., Talbert, J., de Klerk, A., Zippel, S., Guerra, M., & Kilcher, L. (2015). Turbulence measurements from moving platforms. Presented at Currents, Waves, and Turbulence Measurements Workshop. St. Petersburg, FL.

4.2 University Students

- Robert J. Cavagnaro, University of Washington, Seattle, WA, Ph.D. candidate.
- Dominic Forbush, University of Washington, Seattle, WA, Ph.D. student.
- Maricarmen Guerra, University of Washington, Seattle, WA, Ph.D. student. Her work was independently funded by a Fulbright Fellowship.

4.3 Interns

- Matt Wilson, Dartmouth College, Hanover, NH, B.S., mechanical engineering, 2016.
- MacKenzie Sullivan, University of Southern Maine, Portland

5 Computer Modeling

5.1 Model Description, Key Assumptions, Version, Source and Intended Use

Models were created to simulate various control schemes and implementation. These models are SIMULINK models within the MatLab environment. The models predict the transient behavior of the system with given system parameters and inputs provided by the user.

The models are provided in the Marine Hydrokinetic Data Repository as a data deliverable from this project.

5.2 Performance Criteria for the Model Related to the Intended Use

The simulation models were intended primarily to investigate the performance of candidate control schemes from a qualitative and quantitative perspective. As the full system is inherently much more complex than can be modeled with the lumped parameter system approach used in the SIMULINK models, simplifications are required to achieve a working model. These simplifications naturally reduce the fidelity of the models.

After consultation with team members it was decided that the performance criteria to be selected to compare model with each other and with empirical data would be a quantity defined as the *Energy Loss (E Loss)*. This represented the fraction of energy lost due to ineffectiveness of the control scheme. A perfect control scheme would achieve an *E Loss* value of zero.

This performance criterion proved effective in comparing analytical predictions between different control system models and as such was valuable. However the final results of the modeling effort delivered control schemes with little measureable difference between *E Loss* values for the differing control schemes. This implied that the expected difference between the schemes in the field should be negligible. Data from the testing effort showed qualitative differences between the implemented controls schemes. These qualitative differences were primarily related to the stability of the particular control schemes in given regimes, with significant differences between predicted capabilities and actual capabilities. Some control schemes were inherently unstable in operation while being predicted to be stable in models. The reasons for these deviations are multiple and are discussed above. Primary reasons for the discrepancy are due to the assumption that noise within the simulation input water speed series from ADV data was fully reflective of the real world water speed distribution; and assumption that the turbine could be assumed to produce a constant torque with no torque ripple for a constant water speed. This assumption may prove to be inaccurate and a consideration of torque ripple may improve the fidelity of the models.

In simulation and flume testing the *E Loss* factor proved capable of distinguishing performance of control schemes. However in the emulator and field tests the *E Loss* factor did not prove to be a particularly effective performance criteria to distinguish between quantitative behavior of control schemes at given set points. Noise in the empirical data tended to larger than the predicted variation between *E Loss* values.

5.3 Test Results to Demonstrate The Model Performance Criteria Were Met

Testing of the simulation models was performed against tow tank models by University of Washington, and against empirical data collected during the course of this project.

5.4 Theory behind the Model, Expressed in Non-Mathematical Terms

Feed forward control schemes were modeled. Feed forward control is a term describing an element or pathway within a control system which passes a controlling signal from a source in its external environment, often a command signal from an external operator, to a load elsewhere in its external environment. A control system which has only feed-forward behavior responds to its control signal in a pre-defined way without responding to how the load reacts; it is in contrast with a system that also has feedback, which adjusts the output to take account of how it affects the load, and how the load itself may vary unpredictably; the load is considered to belong to the external environment of the system.

In a feed-forward system, the control variable adjustment is not error-based. Instead it is based on knowledge about the process in the form of a mathematical model of the process and knowledge about or measurements of the process disturbances.

5.5 Mathematics to be Used, Including Formulas and Calculation Methods

SIMULINK uses

5.6 Whether or not the Theory and Mathematical Algorithms Were Peer Reviewed

Feed forward control theory has been extensively reviewed[1]
The benefits of feed forward control are significant and can often justify the extra cost, time and effort required to implement the technology. Control accuracy can often be improved by as much as an order of magnitude if the mathematical model is of sufficient quality and implementation of the feed forward control law is well thought out. Energy consumption by the feed forward control system and its driver is typically substantially lower than with other controls. Stability is enhanced such that the controlled device can be built of lower cost, lighter weight while still being highly accurate and able to operate at high speeds. Other benefits of feed forward control include reduced wear and tear on equipment, lower maintenance costs, higher reliability and a substantial reduction in hysteresis.

5.7 Hardware requirements

Personal computer

5.8 Documentation

READ ME files are provided as part of the simulation codes.

6.0 References

Bachant, P., Wosnik, M., Gunawan, B., Neary,V.S , *Experimental Study of a Reference Model Vertical-Axis Cross-Flow Turbine,* Submitted for publication, Under Review

Brabandere, K, De., *A voltage and frequency droop control method for parallel inverters*, IEEE Annual Power Electronics Specialist Conference, 4:2501 - 2507 VOL 4.(2004)

Cavagnaro, R.J., Neely, J.C., Fay, F.-X., Mendia, J.L., & Rea, J.A., *Evaluation of Electromechanical Systems Dynamically Emulating a Candidate Hydrokinetic Turbine*," Sustainable Energy, IEEE Transactions on , vol.7, no.1, pp.390-399. doi:10.1109/TSTE.2015.2492943

Fey, U., König, M., & Eckelmann, H. (1998). A new Strouhal–Reynolds-number relationship for the circular cylinder in the range $47<Re<2\times10^5$. Physics of Fluids, 10(7), 1547. doi:10.1063/1.869675

Forbush, D., Polagye, B., Thomson, J., Fabien, B., Donegan, J., & McEntee, J. (2015). Characterization and control of a cross-flow turbine in shear flow. In *Proceedings of the 3rd Marine Energy Technology Symposium* (pp. 3–8). Washington, D.C.

Ginter, V. J., & Pieper, J. K. (2011). Robust Gain Scheduled Control of a Hydrokinetic Turbine. *IEEE Transactions on Control Systems Technology*, *19*(4), 805–817.

Haugen, F. (2009). Basic Dynamics and Control. ISBN 978-82-91748-13-9

Jenne, D.S., *Ocean Renewable Power Company Baseline LCOE: DOE Advanced Controls*, NREL Technical report, March 2016.

Kilcher, L., Thomson, J. & Colby, J. (2014).*Determining the spatial coherence of turbulence at MHK sites*, Proceedings of the 2nd Marine Energy Technical Symposium (METS), 2014.

Pao, L. Y., & Johnson, K. E. (2011). *Control of Wind Turbines*. IEEE Control Systems, 31(2), 44–62. doi:10.1109/MCS.2010.939962

Thomson, J. (2012). Observations of wave breaking dissipation from a SWIFT drifter, *J. Atmos. & Ocean. Tech.,* 29.

Thomson, J., Polagye, B.,Durgesh, V. &Richmond, M. (2102). Measurements of turbulence at two tidal energy sites in Puget Sound, WA, J. Ocean. Eng., 37 (3), 363–374

Thomson, J., L. Kilcher, M. Richmond, J. Talbert, A. deKlerk, B. Polagye, M. Guerra, and R. Cienfuegos, *Tidal turbulence spectra from a compliant mooring*, Proceedings of the 1st Marine Energy Technical Symposium (METS), 2013.

Thomson, J., M. Richmond, B. Polagye, V. Durgesh, Measurements of turbulence at two tidal energy sites*, J. Ocean. Eng.*, **37** (2012).